

Pharmacological GLI2 inhibition prevents myofibroblast cell-cycle progression and reduces kidney fibrosis

Rafael Kramann,^{1,2} Susanne V. Fleig,^{1,3} Rebekka K. Schneider,⁴ Steven L. Fabian,¹ Derek P. DiRocco,¹ Omar Maarouf,¹ Janewit Wongboonsin,¹ Yoichiro Ikeda,¹ Dirk Heckl,⁴ Steven L. Chang,⁵ Helmut G. Rennke,⁶ Sushrut S. Waikar,¹ and Benjamin D. Humphreys^{1,7}

¹Renal Division, Brigham and Women's Hospital, Department of Medicine, Harvard Medical School, Boston, Massachusetts, USA. ²Division of Nephrology and Clinical Immunology, RWTH Aachen University Medical Faculty, RWTH Aachen University, Aachen, Germany. ³Division of Nephrology and Hypertension, Hannover Medical School, Hannover, Germany. ⁴Division of Hematology, Brigham and Women's Hospital, Department of Medicine, Harvard Medical School, Boston, Massachusetts, USA. ⁵Division of Urology and ⁶Department of Pathology, Brigham and Women's Hospital, Boston, Massachusetts, USA. ⁷Harvard Stem Cell Institute, Cambridge, Massachusetts, USA.

Chronic kidney disease is characterized by interstitial fibrosis and proliferation of scar-secreting myofibroblasts, ultimately leading to end-stage renal disease. The hedgehog (Hh) pathway transcriptional effectors GLI1 and GLI2 are expressed in myofibroblast progenitors; however, the role of these effectors during fibrogenesis is poorly understood. Here, we demonstrated that GLI2, but not GLI1, drives myofibroblast cell-cycle progression in cultured mesenchymal stem cell–like progenitors. In animals exposed to unilateral ureteral obstruction, Hh pathway suppression by expression of the GLI3 repressor in GLI1⁺ myofibroblast progenitors limited kidney fibrosis. Myofibroblast-specific deletion of *Gli2*, but not *Gli1*, also limited kidney fibrosis, and induction of myofibroblast-specific cell-cycle arrest mediated this inhibition. Pharmacologic targeting of this pathway with darinaparsin, an arsenical in clinical trials, reduced fibrosis through reduction of GLI2 protein levels and subsequent cell-cycle arrest in myofibroblasts. GLI2 overexpression rescued the cell-cycle effect of darinaparsin in vitro. While darinaparsin ameliorated fibrosis in WT and *Gli1*-KO mice, it was not effective in conditional *Gli2*-KO mice, supporting GLI2 as a direct darinaparsin target. The GLI inhibitor GANT61 also reduced fibrosis in mice. Finally, *GLI1* and *GLI2* were upregulated in the kidneys of patients with high-grade fibrosis. Together, these data indicate that GLI inhibition has potential as a therapeutic strategy to limit myofibroblast proliferation in kidney fibrosis.

Introduction

The rising incidence of diabetes and hypertension in our aging population has led to increased rates of both chronic kidney disease (CKD) and end-stage renal disease (ESRD) (1–3). Estimates of CKD prevalence approach 10% in the United States, with more than 600,000 patients living with ESRD (3). These patients suffer substantial morbidity and mortality while on dialysis, and kidney transplant wait times number in years, because there are not enough kidneys available. The cost of caring for patients with ESRD also consumes a disproportionate fraction of health care budgets (3). For these reasons, novel therapeutic strategies to slow down CKD progression and reduce the incidence of ESRD are urgently needed.

Kidney fibrosis is the common final pathway for nearly all progressive kidney diseases. Inhibiting kidney fibrosis, therefore, represents a logical strategy to slow the progression of CKD to ESRD. However, there are currently no approved drugs available to treat kidney fibrosis (4). Myofibroblasts are widely accepted as the cell type responsible for the secretion of matrix proteins that drive kidney fibrosis (4, 5), and we have recently shown that GLI1 expression identifies a perivascular mesenchymal stem cell–like

(MSC-like) progenitor population that gives rise to myofibroblasts in solid organ injury (6). Genetic ablation of these cells ameliorates heart and kidney fibrosis, providing a proof of principle for the therapeutic targeting of these cells (6). The specificity of GLI1 expression in these myofibroblast progenitors prompted us to investigate the functional role of the hedgehog/GLI (Hh/GLI) pathway in these cells during fibrosis.

In vertebrates, 3 members of the GLI transcription factor family exist — GLI1, GLI2, and GLI3 — and are likely derived from duplications of a single ancestral *GLI* gene (7). All GLI proteins contain a C-terminal activator domain, whereas only GLI2 and GLI3 possess an N-terminal repressor domain (8). Findings in mouse mutants suggest that GLI2 is important for the activator function in response to Hh signaling, while GLI3 is the major repressor; GLI1 primarily amplifies the transcriptional response (8–12). The Hh receptor patched (PTC) is localized in and around the primary cilium. Upon binding of an Hh ligand (sonic, desert, or Indian Hh), PTC releases tonic inhibition of the transmembrane protein smoothened (SMO) and leaves the cilium. SMO activation results in accumulation of suppressor of fused–GLI2 (SUFU–GLI2) and SUFU–GLI3 complexes in the cilium, which otherwise would have been ubiquitinated and degraded (8, 9, 13). Following dissociation from SUFU, GLI2 — and GLI3 — translocate into the nucleus, where they activate the expression of Hh target genes, including *Gli1* and *Ptc1* (8, 9, 13).

Conflict of interest: The authors have declared that no conflict of interest exists.

Submitted: December 26, 2013; **Accepted:** June 4, 2015.

Reference information: *J Clin Invest*. 2015;125(8):2935–2951. doi:10.1172/JCI74929.

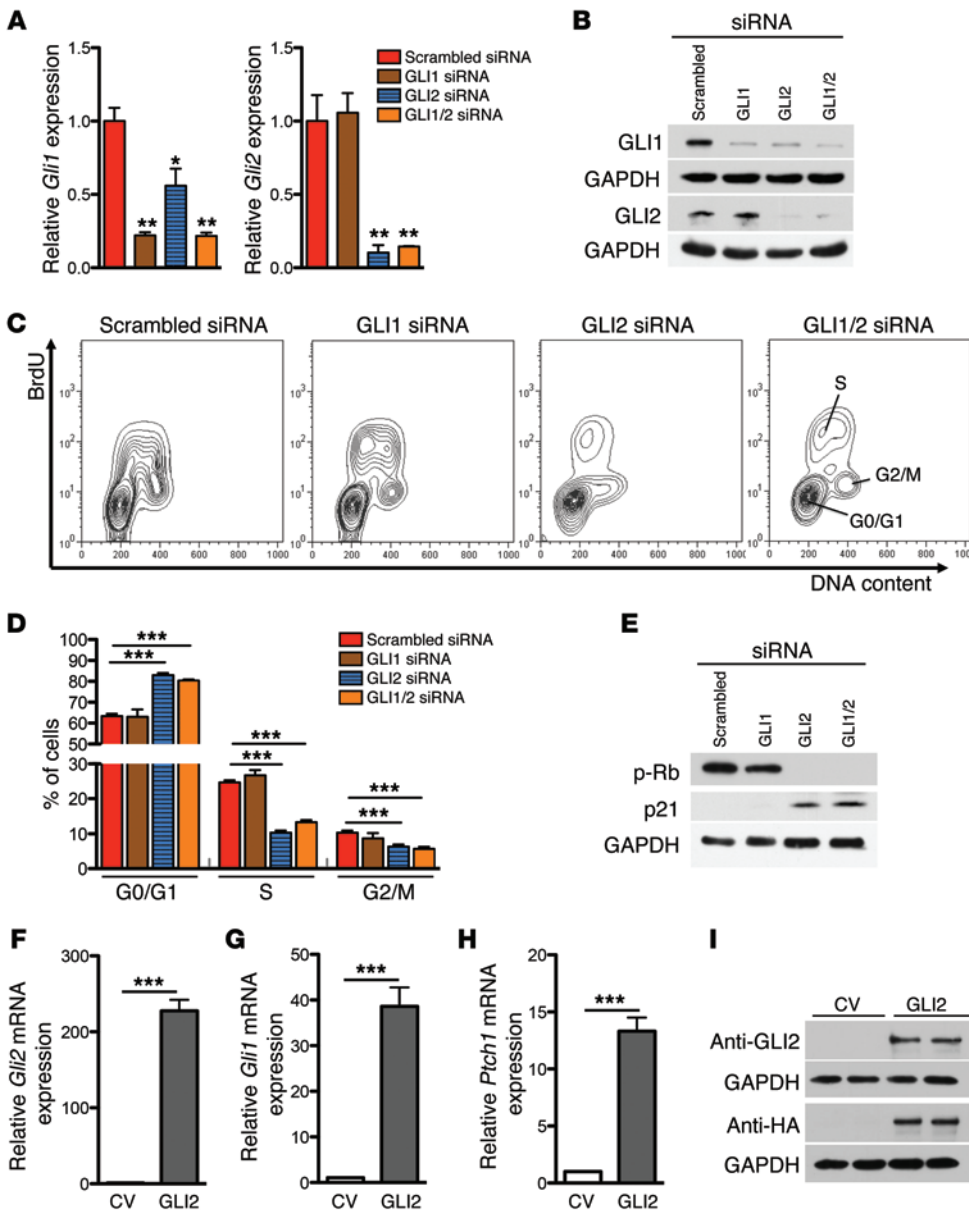


Figure 1. Lowering GLI2, but not GLI1, levels by RNAi induces cell-cycle arrest of MSC-like cells in vitro. (A and B) mRNA and protein levels of GLI1 and GLI2 in 10T1/2 cells treated with siRNA, as indicated. Shh was added to the medium to increase GLI protein levels for better detection ($n = 3$ biological replicates). Quantification of Western blot data from 3 replicates is shown in Supplemental Figure 1. (C and D) Representative flow cytometric cell-cycle plots and quantification of 10T1/2 cells after siRNA-mediated knockdown of GLI1, or GLI2, or both GLI1 and GLI2, compared with scrambled siRNA ($n = 3$ replicates). (E) Representative Western blot of cell-cycle regulators at the G1 restriction point p-Rb and p21 following knockdown of GLI1, GLI2, or GLI1/2. Quantification of Western blot data from 3 replicates is shown in Supplemental Figure 1. (F–I) Overexpression of GLI2 by retroviral delivery activates the Hh pathway, with increased downstream expression of GLI1 and PTCH1. * $P < 0.05$, ** $P < 0.01$, and *** $P < 0.001$, by t test (A) or 1-way ANOVA followed by Bonferroni' post-hoc test (D). Data represent the mean \pm SEM.

In mammals, GLI1 is not required for sonic hedgehog (Shh) signaling, and *Gli1*-KO mice develop normally, unless 1 copy of *Gli2* is defective (12, 14), whereas *Gli2*-KO mice die at birth with severe skeletal and neural defects (15, 16). Studies in mutant mice, in which the zinc finger–encoding exons have been removed from either *Gli1* or *Gli2* genes, suggest that GLI2 can rescue most GLI1 functions, whereas GLI1 cannot rescue GLI2 function (12). Interestingly, when GLI1 is expressed from the endogenous *Gli2* locus, it can rescue the in vivo function of GLI2, suggesting that only the activator form of GLI2 is required for development (17).

The Hh pathway regulates mesenchymal cell fates during kidney and ureteric development, and growing evidence implicates a critical role of Hh in solid organ fibrosis and cancer (4, 5, 8, 18, 19). We and others have reported a role of the Hh pathway in renal fibrosis (20–22). While some evidence suggests an upregulation of Hh ligands during kidney fibrosis, accumulating data indicate that GLI proteins can also be activated in a ligand-independent fash-

ion by TGF- β (23, 24), PDGF (25, 26), EGFR, RAS, and AKT/PI3K signaling pathways (27–32), all of which have also been reported to contribute to the progression of fibrosis.

Given the specific expression of GLI1 and GLI2 in myofibroblasts and their precursors (6, 20), the important role of Hh signaling in cell proliferation (26, 33, 34), and the possibility of direct activation of GLI proteins by known profibrotic pathways, we investigated the role of GLI1 and GLI2 in myofibroblast function in kidney fibrosis. We demonstrate that conditional KO of *Gli2* or inhibition of GLI proteins by overexpression of the GLI3 repressor in *Gli1*⁺ myofibroblast precursors, but not KO of *Gli1* alone, induces a specific myofibroblast cell-cycle arrest with reduced fibrosis. Furthermore, direct targeting of GLI proteins with darinaparsin, a novel organic arsenical with optimized pharmacokinetic properties that is currently undergoing clinical studies in hematologic malignancies and solid tumors (35, 36), inhibits the Hh effectors GLI1 and GLI2 during kidney fibrosis and prevents myofibroblast prolifer-

eration. Darinaparsin acts by directly binding to GLI2 and inducing a GLI-dependent cell-cycle arrest in kidney myofibroblasts. GANT61, a small-molecule inhibitor of GLI, also ameliorates renal fibrosis in mice, even when administered after injury. Furthermore, we demonstrate that *GLI1* and *GLI2* expression is also increased in fibrotic human kidneys, suggesting that a similar mechanism might be involved in human kidney fibrosis progression.

Results

Knockdown of *GLI2*, but not *GLI1*, induces G0/G1 cell-cycle arrest in vitro. There are many examples of Hh-dependent regulation of cell proliferation in development and disease (9, 26, 33, 37–39). *Gli2*^{-/-} skin transplants are characterized by growth arrest in hair follicle development, while constitutively active GLI2 induces skin proliferation in *Shh*-null mice, suggesting that GLI2 is the effector of Hh-induced proliferation (38). Our own recent data indicate that pharmacologic inhibition of GLI proteins reduces the self-renewal capacity of GLI1⁺ MSC-like myofibroblast precursors (6). To evaluate the role of GLI1 versus GLI2 in cell proliferation in vitro, we performed siRNA-knockdown experiments in the MSC-like cell line 10T1/2 (Figure 1 and Supplemental Figure 1; supplemental material available online with this article; doi:10.1172/JCI74929DS1). Treatment with siRNA directed against GLI1 reduced mRNA and protein levels of GLI1 alone, while siRNA directed against GLI2 reduced both GLI1 and GLI2 expression, consistent with GLI1 as a downstream transcriptional target of GLI2 (Figure 1, A and B, and Supplemental Figure 1, B and C). Flow cytometric analysis of cell-cycle distribution revealed that knockdown of GLI2 (or both GLI1 and GLI2) resulted in G0/G1 arrest, with fewer cells in the S and G2/M phases, whereas siRNA directed against GLI1 alone had no effect (Figure 1, C and D). Knockdown of GLI2, or both GLI1 and GLI2, reduced phosphorylated retinoblastoma (p-Rb, Ser780) levels, with increased levels of the cyclin-dependent kinase inhibitor p21, suggesting that cells exited the cell cycle at the G1 restriction point (Figure 1E and Supplemental Figure 1, D and E).

Overexpression of *GLI2* drives cell proliferation. We next investigated whether overexpression of GLI2 by retroviral delivery (Supplemental Figure 2, A–D) drives proliferation and could rescue the effect of siRNA knockdown. As expected, GLI2 overexpression caused activation of the Hh pathway, which was reflected by increased mRNA expression of *Gli1* and *Ptch1* (Figure 1, F–I). Importantly, GLI2 overexpression increased cell proliferation and was able to rescue the effect of GLI2 or GLI1 and GLI2 knockdown by RNAi, confirming the specificity of the siRNA approach and pointing toward GLI2 as a key regulator of cell proliferation (Supplemental Figure 2, E and F).

Conditional KO of *Gli2* or overexpression of the *GLI3* repressor in *GLI1*⁺ cells reduces kidney fibrosis, but KO of *GLI1* has no effect. Interstitial myofibroblasts and their perivascular precursors are the only cells in the mouse kidney that express GLI1 and GLI2 (6, 20), and it has been reported that KO of *Gli1* ameliorates kidney fibrosis in mice (21). Since GLI2 can compensate for GLI1 function in development, we asked whether conditional KO of *Gli2* in GLI1⁺ cells would provide further additive protection against fibrosis compared with *Gli1* KO alone. To repress the entire GLI family, we also crossed *Gli1-CreER*² mice with the *R26-Gli3T* strain (herein referred to as

Gli3T), in which the GLI3 repressor is expressed from the *Rosa26* locus following Cre-mediated recombination (40). Unilateral ureteral obstruction (UUO) experiments in *Gli1*^{nLacZ} and *Gli2*^{nLacZ} mice and costaining for α -smooth muscle actin (α -SMA) and β -gal confirmed that expression of GLI1 and GLI2 is restricted to the myofibroblast lineage after kidney injury (Supplemental Figure 3, A and B). Western blot analysis of whole-kidney lysates after sham and UUO surgery confirmed the upregulation of endogenous GLI1 and GLI2 protein after kidney injury (Supplemental Figure 3C).

WT littermates, *Gli1*-KO, conditional *Gli2*-KO (*Gli1-CreER*² *Gli2*^{fl/fl}), *Gli1/2*-KO, or *Gli3T* mice were injected with tamoxifen as indicated in Figure 2A, underwent UUO surgery, and were sacrificed on day 10 following UUO (Figure 2A).

As expected, *Gli1*-KO mice lacked GLI1 expression (Figure 2, B–D, and Supplemental Figure 4). *Gli2*-KO and *Gli3T* mice showed substantially reduced expression of GLI1, suggesting that upstream GLI2 regulates basal GLI1 levels. *Gli2*-KO, *Gli1/2*-KO, and *Gli3T* mice exhibited significantly reduced expression of GLI2 compared with levels detected in *Gli1*-KO mice, where GLI2 levels were unaffected (Figure 2, C and D, and Supplemental Figure 4). While *Gli2*-KO, *Gli1/2*-KO, and *Gli3T* mice showed reduced fibrosis severity, KO of *Gli1*, surprisingly, had no appreciable effect when compared with the fibrosis severity observed in WT littermates (Figure 2, E–H, and Supplemental Figure 4). These data indicate that KO of *Gli1* in the presence of GLI2 had no effect on kidney fibrosis, while inhibition of both GLI1 and GLI2 by *Gli3T* or conditional KO of *Gli2* (in haploinsufficient *Gli1*-KO mice) reduced fibrosis severity. These observations are in line with previous reports that *Gli1*-KO mice show no developmental phenotype in the presence of GLI2 (12, 14), suggesting that GLI2 may rescue GLI1 functions, while GLI1 cannot rescue GLI2 function in the absence of GLI2.

A possible explanation for *Gli1* KO being unprotective following UUO in our hands is the different background of the *Gli1-CreER*² mice compared with that of the *Gli1*^{nLacZ} mice previously used to knock out *Gli1* (21). We therefore used *Gli1*^{nLacZ} mice to knock out *Gli1*; however, again, we could not detect a difference in fibrosis severity when comparing *Gli1*^{nLacZ/nLacZ} mice with their WT littermates (Supplemental Figure 5).

Conditional KO of *Gli2* or expression of the *GLI3* repressor in *GLI1*⁺ cells halts kidney fibrosis progression by inducing myofibroblast-specific cell-cycle arrest. Since our in vitro data suggested that GLI2 is required for cell-cycle progression in MSC-like cells, we next asked whether *Gli2* KO or *Gli3T* expression reduces fibrosis severity by halting myofibroblast cell-cycle progression in vivo. WT littermates, *Gli1*-KO, *Gli2*-KO, *Gli1/2*-KO, and *Gli3T* mice received tamoxifen, underwent UUO surgery, and were euthanized on day 3 after surgery. BrdU was administered 3 hours before sacrifice. We performed costaining for BrdU (S phase) with phosphohistone H3 (p-H3) (G2/M phase) and α -SMA (myofibroblasts, Figure 3A). Quantification of stained tubular epithelial cells and interstitial α -SMA⁺ cells revealed a G0/G1 cell-cycle arrest specifically in the interstitial α -SMA⁺ cell population (myofibroblasts) of *Gli2*-KO, *Gli1/2*-KO, and *Gli3T* mice (Figure 3B). Costaining and quantification of α -SMA⁺ with Ki67 confirmed these findings and indicated fewer cycling myofibroblasts after conditional KO of *Gli2* (*Gli2*-KO; *Gli1/2*-KO) or *Gli3T* expression (Supplemental Figure 6,

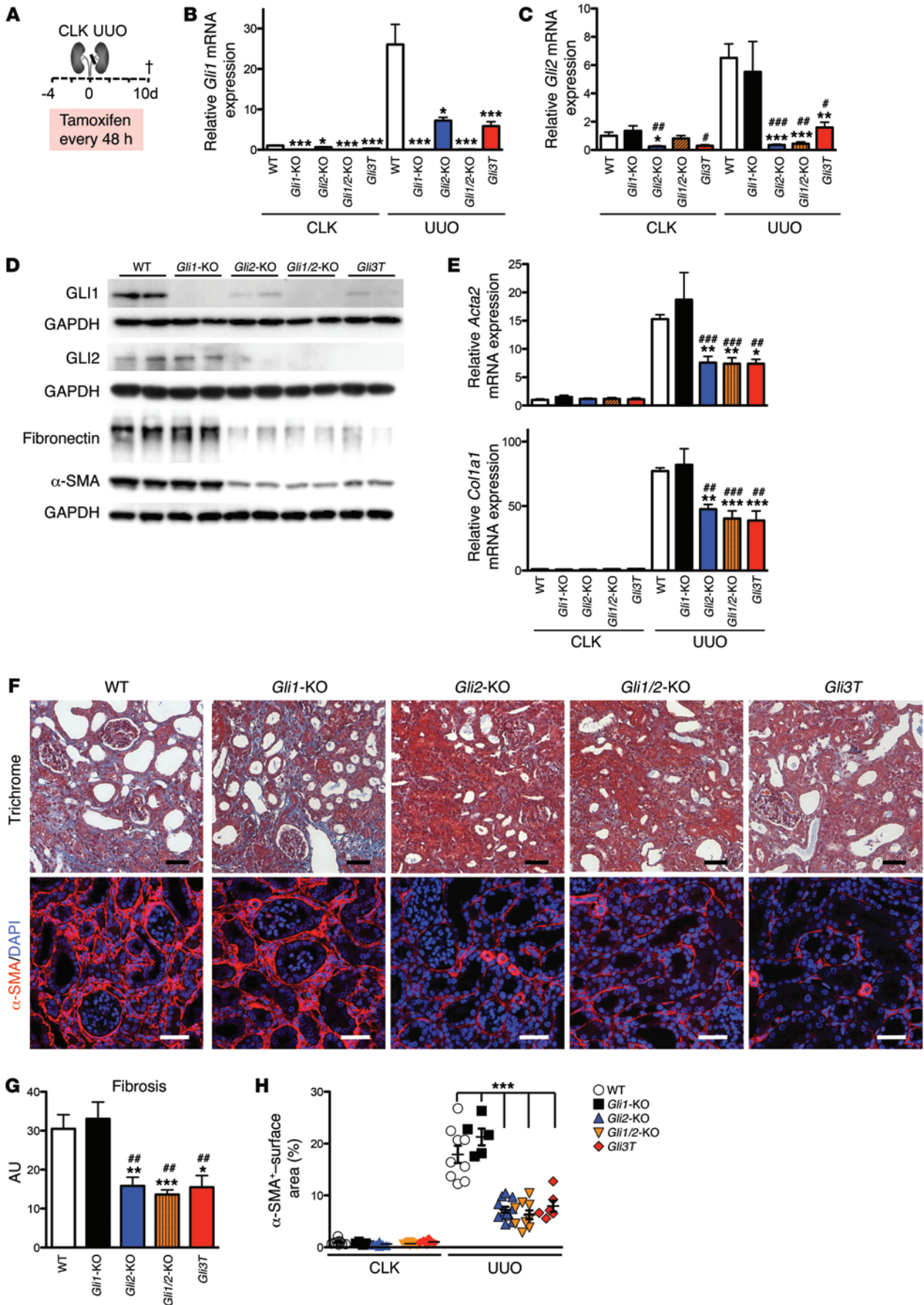


Figure 2. Conditional KO of *Gli2* or overexpression of the GLI3 repressor in GLI1⁺ cells ameliorates kidney fibrosis following UO. (A) WT littermates ($n = 9$, 5 males), *Gli1*-KO ($Gli1^{CreERT2/CreERT2} Gli2^{fl/fl}$; $n = 5$, 3 males), conditional *Gli2*-KO ($Gli1^{CreERT2/+} Gli2^{fl/fl}$; $n = 12$, 7 males), *Gli1/2*-KO ($Gli1^{CreERT2/CreERT2} Gli2^{fl/fl}$; $n = 9$, 5 males), or *Gli3T* ($Gli1^{CreERT2/+} Rosa26-Gli3T$; $n = 6$, 4 males) mice were injected with tamoxifen, underwent UO surgery as indicated, and were sacrificed 10 days after UO. All Tg mice underwent surgery at 8 to 10 weeks of age and can be considered as being on a mixed C57BL/6J and 129SvEv background. WT controls were littermates of the Tg mice used in the experiments. (B and C) qRT-PCR analysis of *Gli1* and *Gli2* mRNA levels in whole-kidney lysates from conditional-KO experiments. (D) Western blots for GLI1 effector proteins and fibrotic readouts fibronectin and α -SMA in UO kidneys. Representative Western blots for the CLKs and quantification by integrated OD (IOD) are presented in Supplemental Figure 4. (E) qRT-PCR analysis of mRNA expression of fibrotic readouts α -SMA (*Acta2*) and collagen1a1 (*Col1a1*). (F) Representative images of trichrome- or α -SMA-stained UO kidneys on day 10 after surgery. (G and H) Quantification of interstitial fibrosis and α -SMA⁺ surface area. * $P < 0.05$, ** $P < 0.01$, and *** $P < 0.001$ versus WT and # $P < 0.05$, ## $P < 0.01$, and ### $P < 0.001$ versus *Gli1*-KO, by 1-way ANOVA followed by Bonferroni's post-hoc test. Data represent the mean \pm SEM.

A–C). Importantly, cell-cycle distribution of tubular epithelial cells or interstitial non-myofibroblast cells (α -SMA⁺) was not affected (Figure 3C, Supplemental Figure 6, C and D, and Supplemental Figure 7, A and B), consistent with recombination specifically in interstitial myofibroblasts and their GLI1⁺ precursors.

Protein analysis of whole-kidney lysates showed increased levels of the cyclin-dependent kinase inhibitor p21 and decreased levels of p-Rb following conditional KO of *Gli2* or expression of the GLI3 repressor (Figure 3, D–F, and Supplemental Figure 7C). Together with our quantification of cell-cycle stages in kidney cells, the results suggest that interstitial myofibroblasts left the cell cycle at the G1 restriction point before the phosphorylation of Rb at Ser780 and are consistent with our in vitro findings after siRNA-mediated knockdown of GLI2.

The novel organic arsenic darinaparsin reduces GLI1 and GLI2 protein levels and induces cell-cycle arrest of MSC-like cells in vitro. We were next interested in determining whether this GLI2-dependent profibrotic pathway in kidney myofibroblasts could be targeted therapeutically. Arsenic trioxide (ATO) is used clinically to treat acute promyelocytic leukemia and was recently shown to antagonize both GLI1 and GLI2 (41, 42). We therefore investigated whether darinaparsin (S-dimethylarsino-glutathione), a novel arsenic-based drug with a favorable systemic toxicity profile (43) and currently undergoing clinical studies in hematologic malignancies and solid tumors (35, 36), inhibits the Hh effectors GLI1 and GLI2 and affects the proliferation of MSC-like cells in vitro. Indeed, darinaparsin was recently shown to modulate GLI protein levels in prostate cancer cell lines (44).

The MSC-like, pericyte-like cell line 10T1/2 was treated with darinaparsin or vehicle, and flow cytometric cell-cycle analysis revealed that darinaparsin (0.5 μ M) induced a G0/G1 cell-cycle arrest of 10T1/2 cells in vitro (Figure 4, A and B). We next asked whether darinaparsin treatment of 10T1/2 cells alters GLI protein levels and the regulator proteins of G1/S cell-cycle transition in a manner similar to that seen in our RNAi studies. Western blot analysis revealed that darinaparsin reduced GLI1 and GLI2 protein levels, with a subsequent upregulation of p21 and decreased

levels of p-Rb (Figure 4, C–E, and Supplemental Figure 8, A and B). Interestingly, while darinaparsin treatment decreased *Gli1* mRNA, *Gli2* mRNA levels remained unchanged (Figure 4, F and G), suggesting an effect of darinaparsin on GLI2 protein stability. To evaluate the effect of darinaparsin on GLI2 protein stability, we transfected human 293T cells with a full-length GLI2 (pcDNA3.1-His; ref. 45), added darinaparsin over a time course of 24 to 72 hours, and performed Western blotting to determine GLI2 protein levels. Quantification of these data indicated a significant decrease in GLI2 protein levels over time (Supplemental Figure 8C). Together with our previous RNAi results, these data suggested that the cell-cycle effect of low-dose darinaparsin might be related to its effect on GLI2 protein levels.

Overexpression of GLI2 rescues the cell-cycle inhibitory effect of darinaparsin. Our results identify GLI2 as a critical regulator of mesenchymal cell proliferation, because reduction of GLI2 protein levels by either RNAi, conditional KO, or darinaparsin treatment caused cell-cycle arrest, and overexpression of GLI2 drove proliferation. We next investigated whether overexpression of GLI2 was sufficient to rescue the inhibitory effect of darinaparsin. GLI2 was overexpressed in 10T1/2 cells delivered retrovirally (Figure 1, F–I, and Supplemental Figure 2, A–D), increased cell proliferation, and rescued the cell-cycle effect of darinaparsin treatment (Figure 4, H and I), pointing toward GLI2 as the molecular target of darinaparsin. We next performed siRNA-knockdown experiments in 10T1/2 cells treated with darinaparsin or vehicle (Supplemental Figure 9). While darinaparsin treatment induced a G0/G1 cell-cycle arrest in cells treated with control siRNA or siRNA directed against GLI1, it did not have an appreciable effect on cells treated with siRNA against GLI2 or both GLI1 and GLI2 (Supplemental Figure 9), further confirming a central role for GLI2 in the cell-cycle inhibitory effect of darinaparsin.

Co-IP suggests that darinaparsin might bind GLI2 in vitro. Although these results implicate GLI2 as a target of darinaparsin, and arsenicals are known to antagonize GLI1 and GLI2, arsenic also inhibits a number of other pathways and could have been inhibiting GLI2 indirectly. On the other hand, arsenic has been proposed to bind to thiol groups on critical cysteine residues located in the GLI zinc finger domains (46), by extension of its known binding to zinc fingers of the promyelocytic leukemia protein (47). To test whether darinaparsin directly binds to GLI2, we overexpressed myc-tagged GLI2 (pCS2-MT GLI2 FL) (48) and myc-tagged eGFP (pEGFP-C1-myc, as a control protein) in human 293T cells. After 72 hours, cells were treated overnight with 0.5 μ M darinaparsin or vehicle, and the cell lysate was incubated with glutathione-S-transferase (GST) agarose beads. Since the arsenic in darinaparsin (S-methylarsino-glutathione) is bound to glutathione moieties, we expected that GST would bind the glutathione, allowing pull-down of darinaparsin itself and of any protein bound to the arsenic. Indeed, using this strategy, we observed that GST beads pulled down GLI2 only in the presence of darinaparsin, but not in its absence, suggesting that darinaparsin indeed binds to GLI2 (Figure 4J). Importantly, we did not detect the EGFP control protein in the IP (Figure 4J). This suggested, together with our previous data, that darinaparsin might reduce GLI2 protein stability by a direct effect. However, this experiment cannot rule out that darinaparsin might also bind other zinc finger proteins, includ-

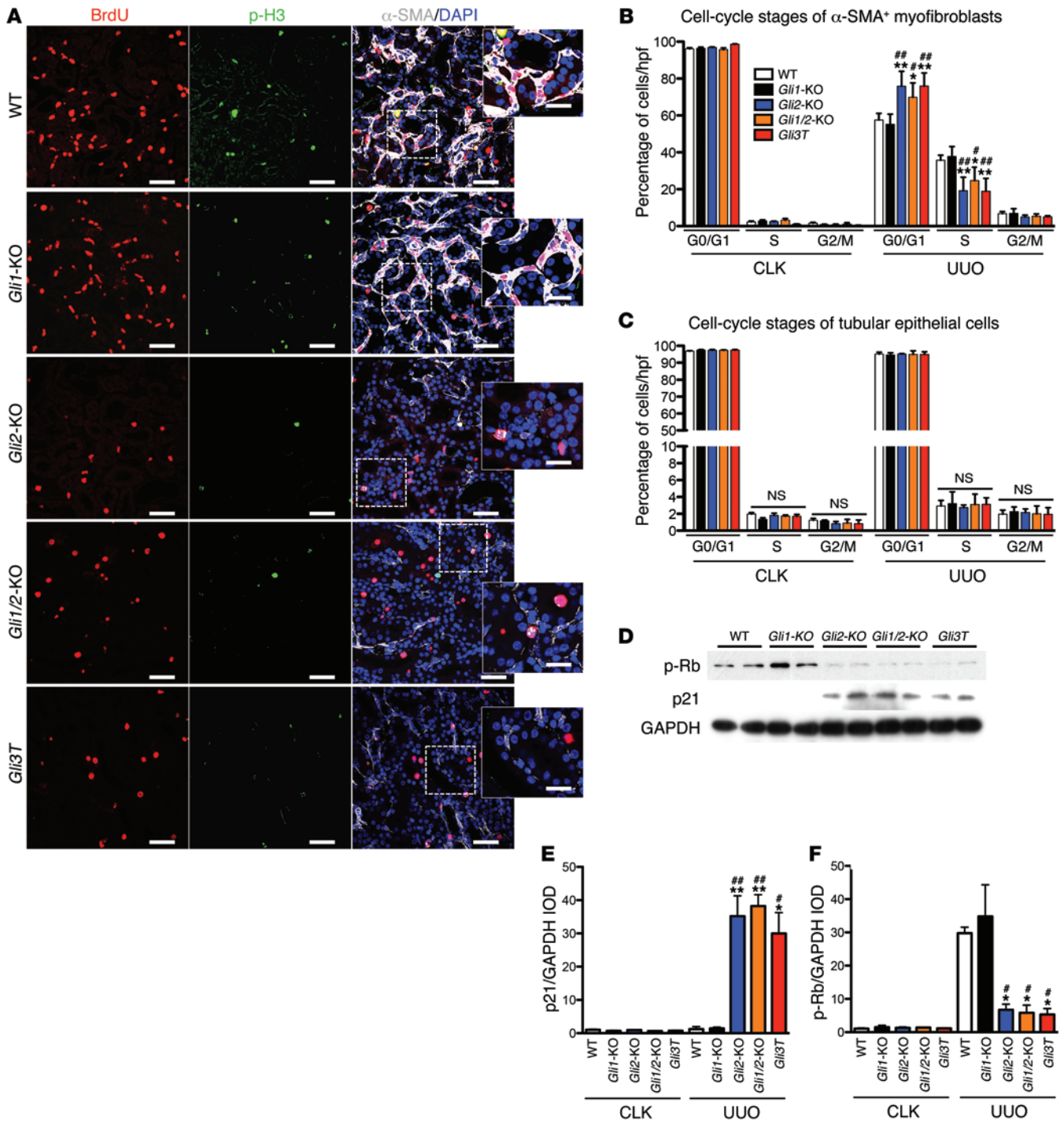


Figure 3. Conditional KO of *Gli2* or overexpression of the GLI3 repressor in GLI1⁺ cells induces myfibroblast-specific cell-cycle arrest. (A) WT littermates, *Gli1*-KO, *Gli2*-KO, *Gli1/2*-KO, and *Gli3T* mice ($n = 5$ /group, 3 males and 2 females/group; mice were on a 129S-C57BL/6J mixed background and were 8–10 weeks of age) received tamoxifen, underwent UUO surgery, and were euthanized on day 3 following surgery. BrdU was administered 3 hours before sacrifice. Representative images of UUO kidneys after costaining for BrdU (S phase), p-H3 (G2/M phase), and α -SMA/myfibroblasts (representative images and quantification of Ki67⁺ cells are shown in Supplemental Figures 6 and 7). Scale bars: 50 μ m, 25 μ m (insets). (B) Cell counting and quantification of myfibroblast cell cycle (S phase = α -SMA⁺/BrdU⁺; G2/M phase = α -SMA⁺/p-H3⁺; G0/G1 phase = α -SMA⁺ - α -SMA⁺/BrdU⁺ - α -SMA⁺/p-H3⁺). (C) Cell counting and quantification of tubular epithelial cell cycle (S phase = tubular epithelial cells [TE] - TE/BrdU⁺; G2/M phase = TE/p-H3⁺; G0/G1 phase = TE - TE/BrdU⁺ - TE/p-H3⁺). (D) Western blot of whole UUO kidney lysates for p-Rb and p21. (E and F) Quantification of Western blots for p-Rb and p21 by IOD. Representative Western blots of noninjured CLKs are shown in Supplemental Figure 7C. * $P < 0.05$ and ** $P < 0.001$ versus WT; # $P < 0.05$ and ### $P < 0.001$ versus *Gli1*-KO, by 1-way ANOVA followed by Bonferroni's post-hoc test. Data represent the mean \pm SEM. hpf, high-power field.

ing GLI1, or that darinaparsin might bind to a second protein that actually binds GLI2. Because reduced GLI2 also causes a reduction in GLI1, we cannot rule out that reduction of both proteins is needed for a cell-cycle effect.

Darinaparsin prevents the increase in GLI1 and GLI2 normally observed during fibrosis and ameliorates fibrosis, even when administered after injury. Having established that darinaparsin lowers GLI protein levels in vitro, we next investigated whether it would reduce the expression of GLI1 and GLI2 in vivo and, most important, reduce the severity of kidney fibrosis. WT mice were treated daily with darinaparsin or vehicle starting 2 days before UUU surgery and sacrificed on day 10 after UUU (Figure 5A). Western blot analysis revealed a significant reduction of endogenous GLI1 and GLI2 protein levels in the UUU kidneys of darinaparsin-treated mice compared with the UUU kidneys in the control group mice (Figure 5B and Supplemental Figure 10). A similar experiment in LacZ reporter mice for GLI1 and GLI2 (*Gli1^{LacZ}*, *Gli2^{LacZ}*) demonstrated that darinaparsin treatment reduced the number of GLI-expressing interstitial cells after UUU (Supplemental Figure 10). Furthermore, darinaparsin treatment resulted in reduced mRNA expression of Hh readouts *Gli1* and *Ptch1* (Supplemental Figure 10).

Strikingly, the severity of fibrosis was significantly reduced in the darinaparsin treatment group (Figure 5, C–G, and Supplemental Figure 11). To determine whether darinaparsin ameliorates fibrosis in a therapeutic rather than preventative dosing strategy, we repeated the UUU experiment but started darinaparsin treatment 2 days after the ureteral ligation surgery. We again observed substantial reductions in fibrotic readouts using this protocol (Supplemental Figure 12, A–F).

To test whether darinaparsin not only improves fibrosis but preserves kidney function in a therapeutic model, we used a severe bilateral ischemia reperfusion injury (IRI) model that causes substantial fibrosis and CKD at 4 weeks, as previously reported as an acute kidney injury (AKI) to CKD model (49). A total of 19 mice underwent surgery and were randomized on day 7 after the surgery to 2 groups, with no difference in their day-1 or day-7 blood urea nitrogen (BUN) levels (Figure 5, H and I, and Supplemental Figure 12I). After randomization, mice were treated daily with darinaparsin or vehicle and sacrificed on day 28 (Figure 5H). Mice in the treatment group showed reduced interstitial fibrosis and reduced expression of fibrotic readouts (Figure 5, J–L, and Supplemental Figure 12). Importantly, the antifibrotic effect of darinaparsin was accompanied by lower BUN and creatinine levels at late time points after injury when compared with the vehicle group (Figure 5I and Supplemental Figure 12J). Our data so far identified darinaparsin as a potentially novel antifibrotic therapy and pointed toward GLI2 inhibition as the molecular mechanism of its action. To prove this, we subjected *Gli1*-KO mice or conditional *Gli2*-KO mice to UUU surgery and treated them with darinaparsin or vehicle starting 2 days before surgery (Supplemental Figure 13). Importantly, darinaparsin treatment ameliorated fibrosis severity in *Gli1*-KO mice, whereas it did not show an appreciable effect on *Gli2*-KO mice (Supplemental Figure 13), confirming a central role of GLI2 in mediating the effect of darinaparsin.

Darinaparsin induces myofibroblast-specific cell-cycle arrest in vivo. Since our previous results indicated that cell-specific KO of

Gli2 led to myofibroblast-specific cell-cycle arrest, we next sought to determine the effect of darinaparsin treatment on myofibroblast proliferation in vivo. C57BL/6J mice were injected with darinaparsin or vehicle starting 2 days before UUU surgery and sacrificed on day 3. BrdU was administered 3 hours before sacrifice. We performed the same costaining experiments as in the in vivo KO experiments and quantified stained tubular and interstitial α -SMA⁺ myofibroblasts and α -SMA⁻ (non-myofibroblasts) cells to calculate the cell-cycle stages for these cell types (Figure 6, A–D, and Supplemental Figure 14, A–E).

Importantly, darinaparsin treatment resulted in a G0/G1 cell-cycle arrest of interstitial myofibroblasts (Figure 6B), without altering the cell-cycle distribution of other kidney cell types (Figure 6, C and D, and Supplemental Figure 14, A–E), suggesting that myofibroblasts are uniquely sensitive to darinaparsin and consistent with our previous finding that myofibroblasts and their precursors are the only kidney cell type expressing GLI proteins during fibrosis (Supplemental Figure 3 and refs. 6, 20). We also measured the proliferation of kidney cell types in mice treated with darinaparsin or vehicle in a therapeutic regime from days 2 to 10 after UUU surgery (Supplemental Figures 15 and 16). Again, we detected significantly decreased proliferation of interstitial myofibroblasts in the darinaparsin treatment arm, with no appreciable effect on other kidney cells (Supplemental Figures 15 and 16).

Western blot analysis of whole-kidney lysates on day 10 after UUU revealed significantly increased expression of the cyclin-dependent kinase inhibitor p21 in the darinaparsin-treated UUU kidneys compared with the vehicle-treated kidneys (Figure 6, E and F). The upregulation of p21 was accompanied by reduced p-Rb protein (Ser780) levels (Figure 6, E and F, noninjured contralateral kidneys [CLKs], and Supplemental Figure 16D). Together with the determination of cell-cycle stages of different kidney cell types (myofibroblasts, tubular epithelial cells, interstitial non-myofibroblasts), these data suggested that myofibroblasts in darinaparsin-treated UUU kidneys most likely exited the cell cycle at the G1 restriction point. These results are consistent with those of our previous experiments examining the effect of Hh pathway blockade on GLI levels through conditional KO of *Gli2* or expression of the GLI3 repressor, which suggested that the in vivo antifibrotic effect of darinaparsin is indeed mediated through the lowering of GLI2 protein levels, with a subsequent cell-cycle arrest of myofibroblasts.

Treatment with GLI antagonist 61, a specific small-molecule GLI antagonist, ameliorates kidney fibrosis following UUU surgery. Collectively, these results suggest that GLI2 is a novel therapeutic target in kidney fibrosis; however, darinaparsin is an arsenical with an uncertain long-term safety profile, even though it has reduced toxicity when compared with ATO (43, 50). This could complicate efforts to develop darinaparsin as an antifibrotic treatment for patients with CKD. Therefore, we investigated whether targeting of GLI proteins using the specific GLI antagonist 61 (GANT61) might inhibit fibrosis in a manner similar to that of darinaparsin.

Mice underwent UUU surgery and were treated using a therapeutic dosing strategy beginning after surgery, as indicated in Figure 7. Scoring of trichrome-stained sections revealed significantly reduced interstitial fibrosis (Figure 7, B and C). Expression of the fibrotic readouts COL1 α 1, α -SMA, and fibronectin were significantly reduced in the UUU kidneys of GANT61-treated mice when

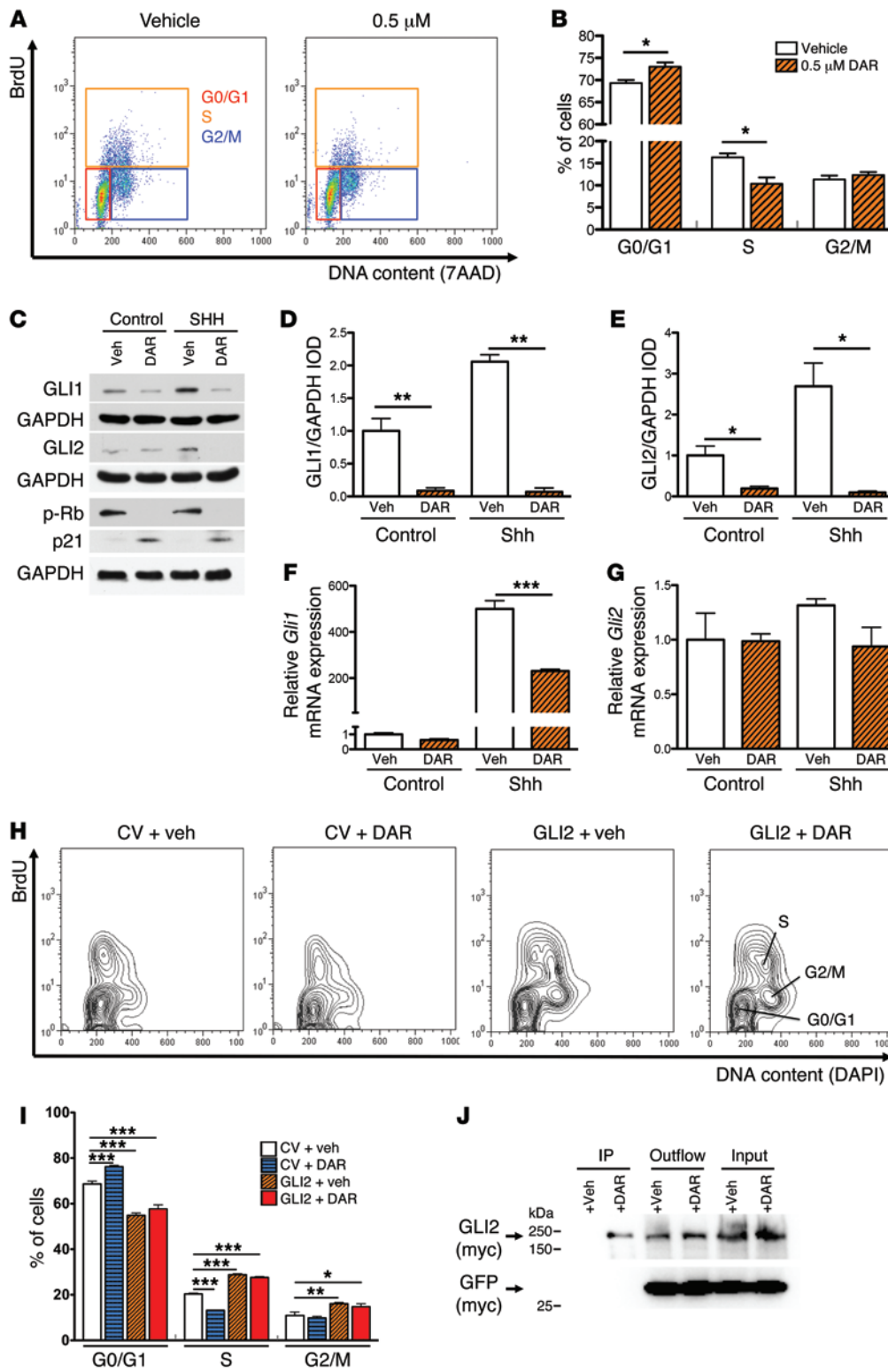


Figure 4. Darinaparsin reduces GLI protein levels and induces cell-cycle arrest in vitro, while overexpression of GLI2 rescues this cell-cycle effect of darinaparsin. (A and B) Darinaparsin induced G0/G1 cell-cycle arrest in the mouse MSC-like, pericyte-like 10T1/2 cell line (BrdU, S phase; 7AAD, 7-amino-actinomycin, DNA content). (C) Representative Western blots of whole-cell lysate from 10T1/2 cells treated with darinaparsin or vehicle in the presence or absence of Shh. Quantification of Western blot analysis for p21 and p-Rb (3 biological replicates) is shown in Supplemental Figure 8. (D and E) Quantification by IOD showing reduced GLI1 and GLI2 protein levels after treatment with darinaparsin (data are from 2 pooled experiments, with a total of 3 biological replicates). (F and G) qRT-PCR analysis of mRNA expression of *Gli1* and *Gli2* in 10T1/2 cells after treatment with vehicle or darinaparsin in the presence or absence of Shh ($n = 3$ replicates). (H and I) Retroviral expression of GLI2 rescued the cell-cycle effect of darinaparsin and drove proliferation of 10T1/2 cells ($n = 3$ biological replicates; gating is shown in Supplemental Figure 2). (J) 293T cells were transfected with full-length GLI2-myc, cotransfected with GFP-myc as a control protein, and treated with darinaparsin or vehicle. GST agarose beads were added to the cell lysate to bind the glutathione moiety of darinaparsin. The immunoblot for myc suggests that in the presence of darinaparsin, GST is able to pull down GLI2 (myc), indicating darinaparsin binding to GLI2 (IP + DAR). Importantly, the GFP-myc control protein was not detectable, indicating the specificity of the IP. * $P < 0.05$, ** $P < 0.01$, and *** $P < 0.001$, by t test (B, D, and F) and by 2-way ANOVA followed by Bonferroni's post-hoc test (I). Data represent the mean \pm SEM. CV, control virus; DAR, darinaparsin; Veh, vehicle.

compared with the UOU kidneys of vehicle-treated mice (Figure 7, D–G). Treatment with GANT61 resulted in significantly reduced GLI1 and GLI2 protein levels in kidneys, accompanied by reduced mRNA expression of the Hh readouts *Gli1* and *Ptch1* (Figure 7, H–N), confirming its ability to antagonize GLI proteins in vivo.

GLI expression is increased in human kidney fibrosis. Given our data on GLI inhibition as a novel antifibrotic therapy in mouse kid-

ney fibrosis, we next asked whether the same pathway might be upregulated in human kidney fibrosis. Fresh tumor nephrectomy specimens were obtained from 10 patients (Supplemental Table 3) and immediately processed for histology and RNA extraction. Fibrosis severity was scored in trichrome-stained sections by a trained kidney pathologist blinded to the mRNA results and clinical details. The kidney specimens were stratified into a low-grade

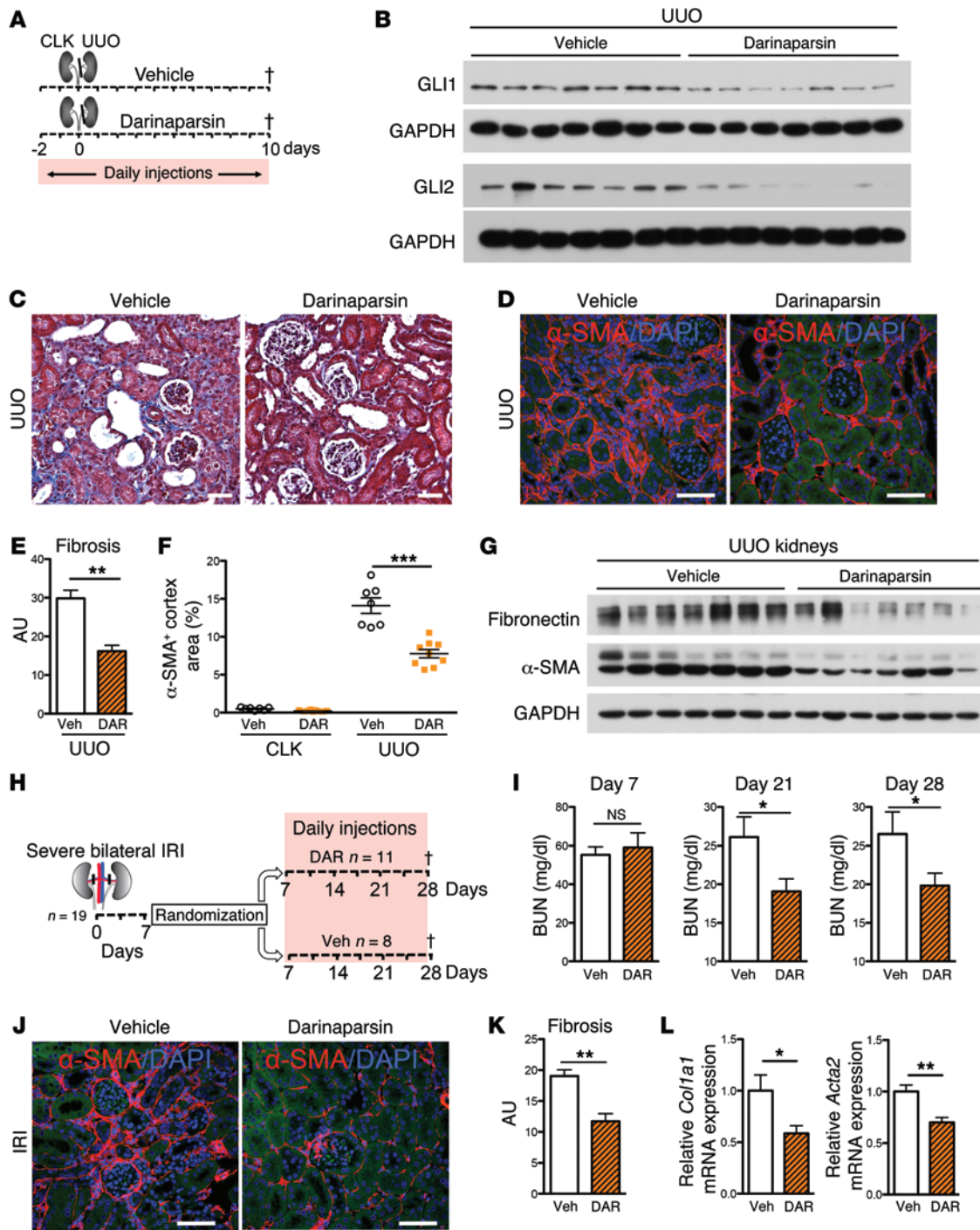


Figure 5. Darinaparsin treatment ameliorates renal interstitial fibrosis after UUU and AKI-to-CKD progression after severe IRI. (A) WT mice (8- to 10-week-old males on a C57BL/6J background) were treated with darinaparsin (50 mg/kg, $n = 9$) or vehicle (normal saline, $n = 7$), as indicated, underwent UUU surgery and were sacrificed on day 10 after surgery. (B) Representative Western blots of whole UUU kidney lysates for GLI1 and GLI2 (Western blots for noninjured CLKs and quantification by IOD are shown in Supplemental Figure 10). (C and D) Representative trichrome-stained and α -SMA-immunostained UUU kidneys. (E and F) Quantification of interstitial fibrosis and α -SMA⁺ surface area. (G) Representative Western blot of whole UUU kidney lysates for fibronectin and α -SMA (Western blots for noninjured CLKs and quantification by IOD are shown in Supplemental Figure 11). (H) WT mice ($n = 19$ male 8- to 10-week-old mice on a C57BL background) underwent severe bilateral IRI and were randomized, on the basis of their day-1 and day-7 BUN levels (Supplemental Figure 12), to darinaparsin or vehicle treatment. (I) BUN measurement at randomization (day 7) and after 14 or 21 days of treatment (BUN levels at baseline and on days 1 and 14, and BW and creatinine data are shown in Supplemental Figure 12). (J) Representative images of α -SMA-immunostained kidneys after IRI. (K) Quantification of interstitial fibrosis ($n = 11$, darinaparsin; $n = 8$, vehicle). (L) Relative mRNA expression for *Col1a1* and *Acta2* ($n = 11$, darinaparsin; $n = 8$, vehicle). * $P < 0.05$, ** $P < 0.01$, and *** $P < 0.001$ versus vehicle-treated mice, by *t* test. Data represent the mean \pm SEM. Scale bars: 50 μ m.

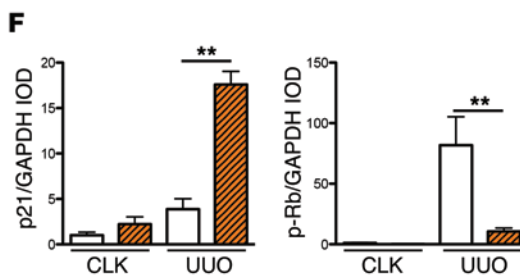
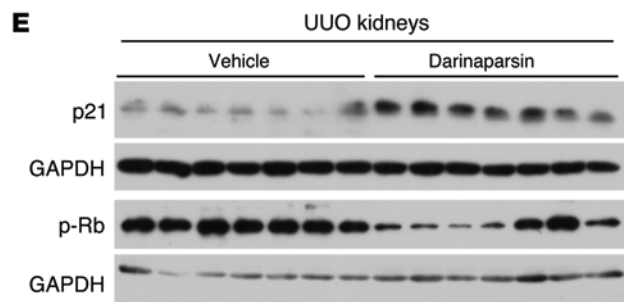
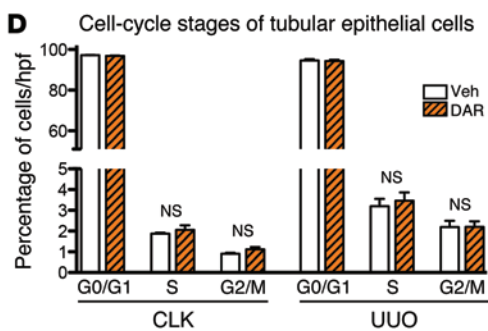
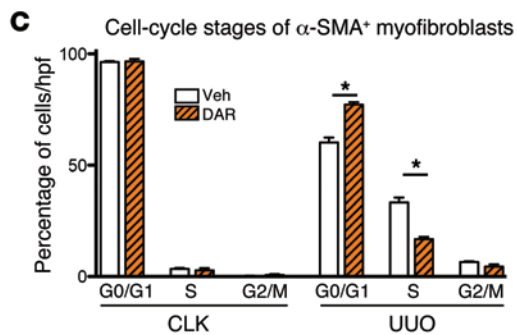
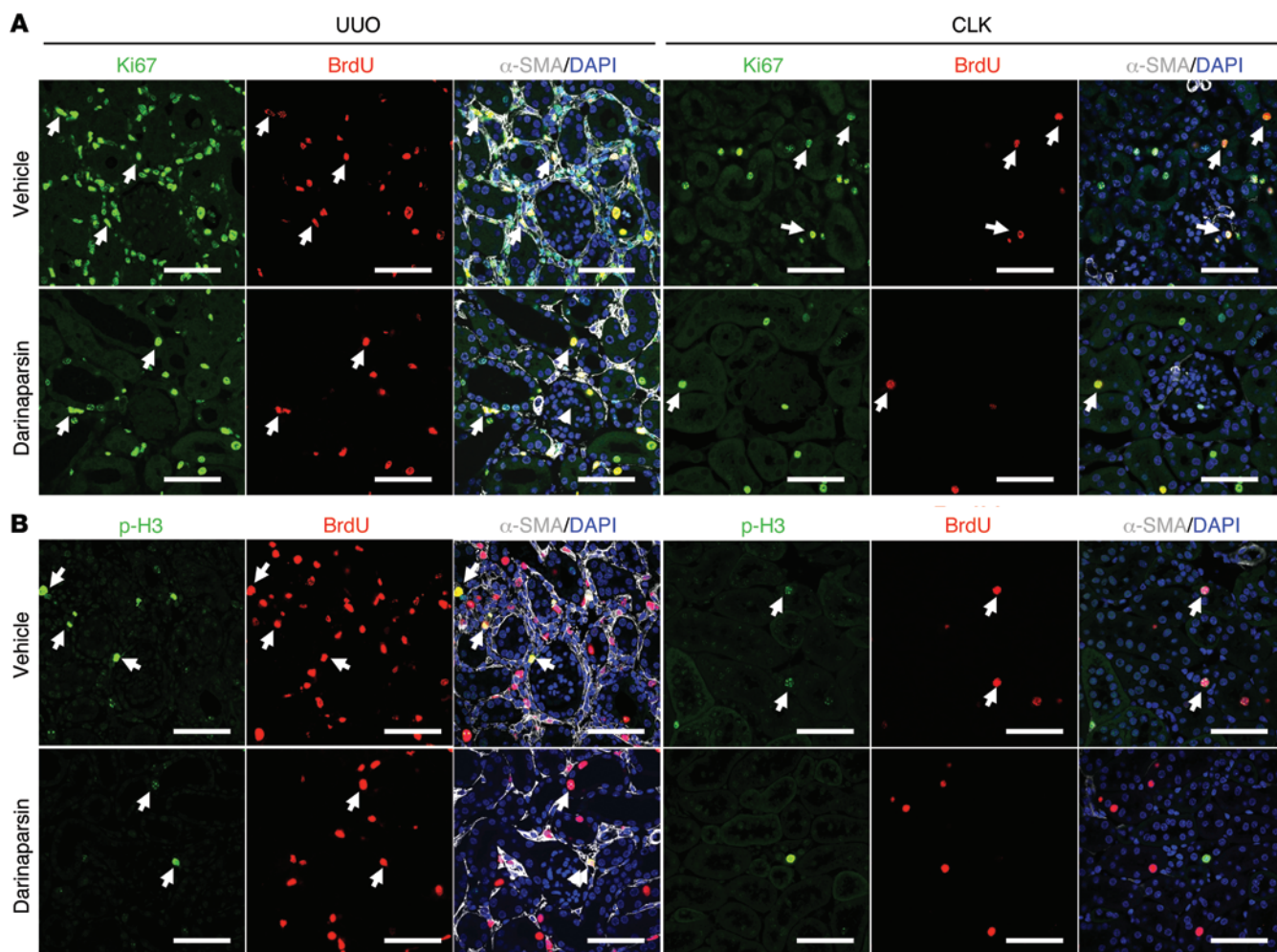


Figure 6. Darinaparsin induces myofibroblast-specific cell-cycle arrest, but does not affect the cell cycle of tubular epithelial cells. Eight- to ten-week-old WT male mice on a C57BL/6J background were treated with darinaparsin (50 mg/kg, $n = 6$) or vehicle ($n = 6$) starting 2 days before UUU surgery and sacrificed on day 3 after surgery. BrdU was injected (100 mg/kg) 3 hours prior to sacrifice. **(A)** Representative images of kidney sections from UUU and noninjured CLKs costained for Ki67, BrdU, and α -SMA, demonstrating reduced proliferation of interstitial myofibroblasts in UUU kidneys of the darinaparsin-treated group compared with the vehicle-treated group. (Quantification of Ki67⁺ cells is shown in Supplemental Figure 14.) **(B–D)** Costaining of sections from noninjured CLKs and UUU kidneys for BrdU (cells in S phase), p-H3 (G2/M phase), and α -SMA allowed quantification of the cell-cycle stages for interstitial myofibroblasts (α -SMA⁺) and tubular epithelial cells. Darinaparsin treatment resulted in a specific G0/G1 cell-cycle arrest of interstitial myofibroblasts in UUU kidneys **(C)**, whereas the cell-cycle distribution of tubular epithelial cells was not effected **(D)**. (A similar analysis was performed in mice treated from day 2 until day 10 after UUU and is shown in Supplemental Figures 15 and 16). **(E and F)** Representative Western blots and quantification by IOD of whole UUU kidney lysates for the cyclin-dependent kinase inhibitor p21/CIP1 and p-Rb (Western blots for noninjured CLKs are shown in Supplemental Figure 16). * $P < 0.05$ by 1-way ANOVA, followed by Bonferroni's post-hoc test **(C)**; ** $P < 0.01$ by t test **(F)**. Data represent the mean \pm SEM. Scale bars: 60 μ m.

fibrosis group (fibrosis grade $\leq 20\%$) and a high-grade fibrosis group (fibrosis grade $\geq 40\%$) (Figure 8, A and B). In line with the histologic scoring, we determined increased mRNA expression of the fibrotic readouts collagen1 α 1 (*COL1A1*), fibronectin (*FN*), and α -SMA (*ACTA2*) in the high-grade fibrosis group (Figure 8C). Importantly, we determined increased expression of *GLI1*, *GLI2*, and *PTCH1* mRNA in the high-grade fibrosis group compared with that detected in the low-grade fibrosis group (Figure 8D). These data suggest activation of the Hh pathway with increased expression of *GLI1* and *GLI2* in human kidney fibrosis (Figure 8).

Discussion

We have recently demonstrated that GLI1⁺ perivascular cells are an important kidney myofibroblast progenitor population (6). Our results herein demonstrate that GLI2 plays a critical functional role in regulating the proliferation of these cells and represent what we believe to be a novel therapeutic target in renal fibrosis. Conditional KO of GLI2 or overexpression of the GLI3 repressor in GLI1⁺ cells ameliorates kidney fibrosis by inducing myofibroblast-specific cell-cycle arrest. The same effects are achieved by GLI2 inhibition via darinaparsin, which we show might directly bind GLI2. Notably, this drug inhibits myofibroblasts specifically and had no appreciable effect on tubular epithelium, consistent with the absence of active Hh/GLI signaling in tubules.

The absence of GLI1 had no effect on kidney fibrosis, in contrast to the report by Ding et al. (21). The reason for this discrepancy is unclear, but we cannot rule out a contribution from the differing mouse backgrounds. On the other hand, our results strongly implicate GLI2 over GLI1 as the critical mediator of profibrotic signaling in kidney, and our findings were consistent across different mouse strains in vivo as well as in our cell culture model. This conclusion confirms previous reports that GLI2 is the major transcriptional activator of Hh signaling and is consistent with the observations that GLI1 is not required for development, whereas *Gli2*-KO mice die at birth (12, 14–16).

ATO is an established therapeutic agent for acute promyelocytic leukemia and acts via degradation of the oncoprotein AML-RXR α (43). Darinaparsin does not act via AML-RXR α degradation, however, and ATO-resistant myeloma cell lines are susceptible to darinaparsin (43). These findings suggest that darinaparsin has a different mechanism of action than does ATO. Darinaparsin, which was designed as an organic arsenic by conjugating dimethylarsenic with glutathione, shows a significantly lower systemic toxicity with a 50-fold higher tolerated maximum dose when compared with ATO (43, 51, 52). Tian et al. reported no significant side effect of darinaparsin on fast-cycling cell populations such as those in the BM or intestine (43). Darinaparsin is currently being tested in phase 2 clinical trials for solid tumors and hematopoietic malignancies; however, its molecular mechanism of action has not been fully elucidated (51). It has been reported that ATO antagonizes both GLI1 and GLI2 (41, 42), and a very recent report also suggests that darinaparsin might reduce GLI2 protein levels in prostate tumor-initiating cells (44).

The mechanism by which arsenicals inhibit GLI2 function is not yet defined, but probably involves effects on protein stability and subcellular localization. Kim et al. analyzed the effect of ATO on Hh signaling on the basis of previous reports that observed a typical Hh-dependent pattern in developing embryos after treatment with arsenic compounds (41, 53–55). They reported that short-term ATO treatment reduces ciliary accumulation of GLI2, leading to Hh pathway inhibition, and that long-term ATO treatment reduced steady-state levels of GLI2, suggesting a direct effect on GLI2 protein stability (41). This is in line with our observation that darinaparsin treatment reduces GLI2 protein levels over time, with a subsequent reduction of downstream GLI1 mRNA and protein expression, whereas *Gli2* gene expression remained unchanged. Our data suggest that darinaparsin might affect GLI2 protein stability by directly binding to GLI2. Importantly, darinaparsin treatment mimics both the cell-cycle effect of RNAi directed against GLI2 in vitro or conditional *Gli2* KO in vivo and induces myofibroblast-specific cell-cycle arrest, with upregulation of p21 and reduction of p-Rb. The cell-restricted expression of GLI1 and GLI2 in kidney myofibroblasts and their precursors might explain the specific effect of darinaparsin on kidney myofibroblasts.

Hh signaling controls the proliferation of diverse cell types during embryogenesis (56, 57) and regulates the proliferation of cancer cells (58–60), and mounting evidence implicates Hh/GLI signaling in cell-cycle progression at the restriction point. In *Drosophila*, Hh signaling induces the expression of cyclin D and cyclin E, both inhibitors of Rb (61). Nagao et al. reported that GLI2 knockdown prevented human osteosarcoma growth by inducing a G1 cell-cycle arrest via upregulation of p21, with a subsequent reduction of Rb phosphorylation (62). Similar effects involving a G0/G1 arrest by upregulation of p21 and reduction of p-Rb have been reported by knockdown of GLI2 in human vascular smooth muscle cells (26), human hepatocellular carcinoma cells (63), and human MSCs (64). All of these findings support our observation that lowering GLI2 protein levels with darinaparsin treatment or siRNA induces cell-cycle arrest of myofibroblasts at the restriction point via p21/CIP1 upregulation, with a subsequent inhibition of Rb phosphorylation, whereas overexpression of GLI2 increases proliferation. Of note, because in all our experiments, lowering

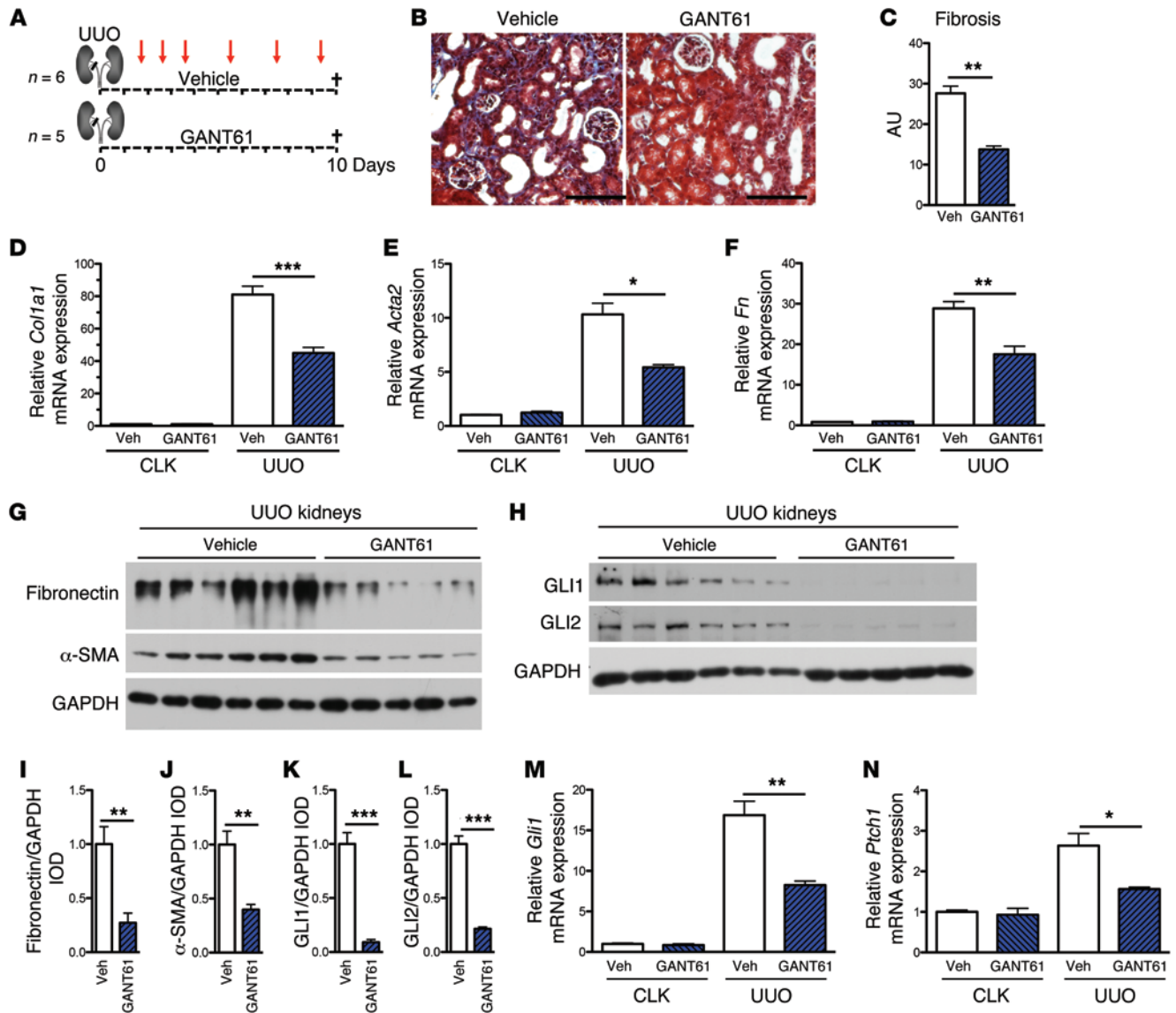


Figure 7. Targeting of GLI proteins by GANT61 ameliorates renal fibrosis following UUO. (A) To test whether specific inhibition of GLI ameliorates renal fibrosis, 8- to 10-week-old male WT mice on a C57BL/6J background were subjected to UUO surgery and treated on the indicated days (arrows) with either GANT61 ($n = 5$) or vehicle (ethanol/corn oil, 1:4; $n = 6$) (50 mg/kg BW, s.c.). (B and C) Trichrome staining and scoring for interstitial fibrosis in UUO kidneys revealed significantly less fibrosis in GANT61-treated mice. (D–F) Determination of mRNA levels revealed significantly lower expression levels of the fibrotic readouts *Col1a1* (D), *Acta2* (E), and fibronectin (*Fn*) (F) in the UUO kidneys of GANT61-treated animals when compared with those of the vehicle-treated animals. (G–L) Representative Western blots and quantification by IOD for fibronectin, α -SMA, GLI1, and GLI2 from whole UUO kidney lysates, demonstrating reduced GLI1 and GLI2 protein expression levels as well as reduced fibrotic readouts. (M and N) GANT61 treatment resulted in a significant reduction in *Gli1* and *Ptch1* mRNA levels following UUO. * $P < 0.05$, ** $P < 0.01$, and *** $P < 0.001$, by *t* test. Data represent the mean \pm SEM. Scale bars: 100 μ m.

GLI2 protein levels always resulted in reduced downstream GLI1 expression, we cannot determine whether the reduction of GLI2 alone, with normal GLI1 levels, would have an appreciable effect. However, our data clearly suggest that inhibition of GLI2, with downstream reduction of GLI1, is a promising therapeutic target in kidney fibrosis.

GANT61 was found in a compound screen to be a direct GLI antagonist with selectivity for the Hh pathway (65). It has been reported that GANT61 induced a G0/G1 arrest, with upregulation of p21 in human colon cancer cells (66). Importantly, in bleomycin-

induced lung fibrosis, GANT61 decreased fibrosis severity, while inhibition of SMO via GDC-0449 did not show this effect (67). Our data demonstrate that directly targeting GLI proteins is a promising therapeutic strategy to treat kidney fibrosis. The ability of a GLI inhibitor that is structurally distinct from darinaparsin to ameliorate fibrosis strongly supports the central role of GLI in kidney fibrosis and as a therapeutic target in CKD.

In conclusion, GLI2 regulates kidney myofibroblast proliferation and is a potential therapeutic target. GLI2 inhibition with a downstream reduction of GLI1, via darinaparsin, reduced fibro-

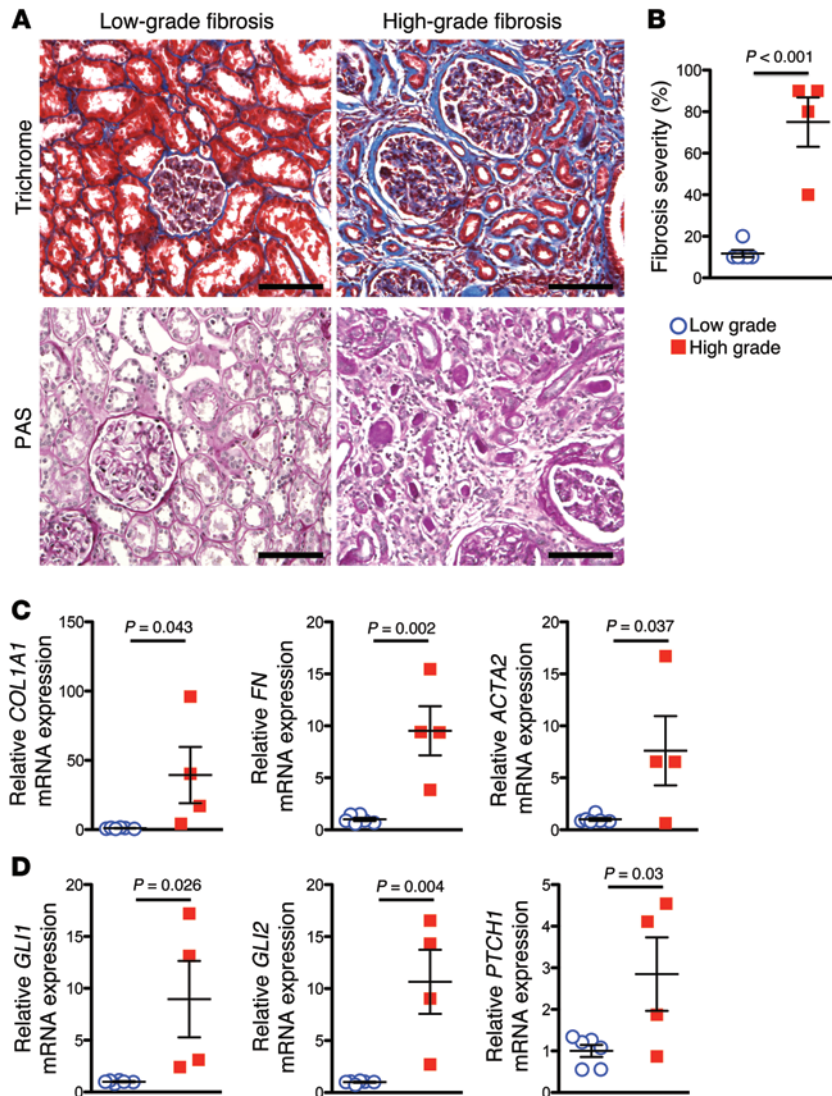


Figure 8. Upregulation of GLI in human kidney fibrosis. (A and B) Human kidney tissue was obtained from tumor nephrectomy specimens from 10 patients and scored by an experienced kidney pathologist for the degree of interstitial fibrosis. (A) Representative images of trichrome and periodic acid-Schiff-stained (PAS-stained) sections of specimens assigned to the high-grade versus low-grade fibrosis groups. (B) Four specimens were assigned on the basis of fibrosis severity to the high-grade fibrosis group (interstitial fibrosis >40%) and 6 specimens to the low-grade fibrosis group (interstitial fibrosis <20%). Clinical data on the patients are provided in Supplemental Table 3. (C) qRT-PCR analysis indicated significantly higher mRNA expression levels of the fibrotic readouts *COL1A1*, *FN*, and *ACTA2* in the high-grade fibrosis group compared with levels in the low-grade fibrosis group, as expected. (D) qRT-PCR analysis indicated a significant upregulation of *GLI1*, *GLI2*, and *PTCH1* mRNA levels in the high-grade fibrosis group compared with that detected in the low-grade fibrosis group. *P* values were calculated by *t* test. Data represent the mean \pm SEM. Scale bars: 100 μ m.

sis in 2 kidney fibrosis models—even when administered after the onset of fibrosis—by decreasing myofibroblast proliferation. Furthermore, antagonizing GLI proteins with GANT61 also ameliorated renal fibrosis, confirming the relevance of GLI proteins in kidney fibrosis and providing a more specific compound with potentially fewer side effects than those of arsenics. Importantly, our data also suggest that this pathway is upregulated in human kidney fibrosis, providing strong support for future investigation of GLI inhibition to slow CKD progression in humans.

Methods

Animal experiments. WT mice used in these experiments were 8- to 10-week-old males on a C57Bl/6J background and were purchased from Charles River Laboratories. *Gli1-CreER²* (i.e., *GLI1tm3(re/ERT2)Alj/J*, JAX stock no. 007913); *Gli2* floxed (i.e., *GLI2^{tm6Alj/J}*, JAX stock no. 007926); *Gli3T* (i.e., *Gt(ROSA)26Sor^{tm3(GLI3)Amc/J}*, JAX stock no. 013124); *Gli1^{nLacZ}* (JAX stock no. 008211); and *Gli2^{nLacZ}* (JAX stock no. 0007922) were purchased from The Jackson Laboratory.

Gli1-KO mice were generated from homozygous *Gli1-CreER²* mice or by breeding heterozygous *Gli1^{nLacZ/+}* (on a 129S1/SvImJ back-

ground) mice that harbored a β -gal knockin at the transcriptional start site that abolishes *Gli1* gene function (14). Offspring were genotyped by PCR according to The Jackson Laboratory protocol. WT littermates were used as controls in the conditional-KO experiments and heterozygous littermates were used as controls for the quantification of LacZ-positive cells. For the conditional-KO experiments, all mice received tamoxifen in corn oil from Cayman Chemical (3% ethanol, 0.4 mg/kg BW, p.o.) as indicated in Figure 2.

All mice underwent UUO surgery at 8 to 10 weeks of age, as previously described (20). Briefly, after flank incision, the left ureter was tied off at the level of the lower pole with two 4.0 silk ties. Mice were sacrificed on day 10 after surgery. For the quantification of cell proliferation, mice were injected with BrdU (Sigma-Aldrich, 100 mg/kg BW in normal saline, i.p.) on day 3 after surgery and sacrificed 3 hours after BrdU injection. LacZ-positive cells in *Gli1^{nLacZ/nLacZ}* versus *Gli1^{nLacZ/+}* mice were quantitated on day 7 after UUO surgery. For the bilateral IRI experiments, surgery was performed as previously described (68). Briefly, mice were anesthetized with pentobarbital sodium (60 mg/kg BW, i.p.), kidneys were exposed through flank incisions, and mice were subjected to ischemia by clamping the renal pedicle with non-

traumatic microaneurysm clamps (Roboz Surgical Instrument Co.) for 26 minutes. Body temperatures were controlled at 36.5°C to 37.5°C throughout the procedure. Mice were bled via the tail vein 7 days prior to surgery and on days 1, 7, 14, 21, and 28 after surgery. BUN levels were measured using the Infinity Urea assay (Thermo Scientific) according to the manufacturer's instructions. Serum creatinine was assessed by HPLC (69) at the O'Brien Core Center for Acute Kidney Injury Research (University of Alabama School of Medicine, Birmingham, Alabama, USA).

Darinaparsin experiments. Darinaparsin (Zio-101; ZIOPHARM Oncology) was freshly prepared by dissolving in normal saline (vehicle) before treatment of cells or animals. For animal experiments, a 5-mg/ml stock solution was prepared, and animals were given a daily i.p. injection of 50 mg/kg BW darinaparsin or vehicle. In the UUO experiments, mice were randomly assigned to the darinaparsin or vehicle group and treated starting 2 days before surgery (Figure 5, A–G) or starting 2 days after surgery (Supplemental Figure 13, A–F). The last dose was given 4 hours before the mice were sacrificed. In the IRI experiment, mice were treated daily starting on day 7 after surgery until they were sacrificed, on day 28 after surgery. For the cell culture experiments a 1-mM stock solution was sterile filtered, and a final concentration of 0.5 to 3 μ M was used in the cell culture medium every 24 hours versus normal saline (vehicle).

GANT61 experiments. GANT61 (catalog 13841; Cayman Chemical) was dissolved in ethanol and stored at –80°C. The ethanol solution was further diluted in corn oil (1:4) immediately before s.c. injection (50 mg/kg BW) on days 1, 2, 3, 5, 7, and 9 after UUO surgery. Preparation of GANT61 in this ethanol/oil solution and delivery via s.c. injection in mice have been described previously by Lauth et al. (70). Control mice were injected with the vehicle (ethanol/corn oil, 1:4) at the same time points.

Tissue preparation and histology. Mice were anesthetized with isoflurane (Baxter) and subsequently perfused via the left ventricle with 4°C PBS for 1 minute. For histological analyses, tissue sections were fixed in 10% formaldehyde for 1 hour, paraffin embedded, cut with a rotating microtome at a thickness of 3 μ m, and stained according to routine histological protocols. For immunofluorescence studies, kidneys were fixed in 4% paraformaldehyde (PFA) on ice for 1 hour, then incubated in 30% sucrose in PBS at 4°C overnight. OCT-embedded (Sakura Finetek) kidneys were cryosectioned into 7- μ m sections and mounted on Superfrost slides (Fisher Scientific). Sections were washed in 1X PBS, blocked in 10% normal goat serum (Vector Laboratories), and incubated with primary Abs targeting BrdU (1:100; catalog ab6326; Abcam); p-H3 (1:100; catalog SC-8656-R; Santa Cruz Biotechnology Inc.); α -SMA (1:200; catalog A2547; Sigma-Aldrich); α -SMA-Cy3 (1:200; catalog C6198; Sigma-Aldrich); Ki67 (1:100; catalog VP-K451; Vector Laboratories); and laminin (1:100; catalog L9393; Sigma-Aldrich). The secondary Abs used were FITC-, Cy3-, or Cy5-conjugated (Jackson ImmunoResearch). Sections were then stained with DAPI and mounted in Prolong Gold (Life Technologies).

Quantification of BrdU⁺ and p-H3⁺ tubular epithelial cells and myofibroblasts (α -SMA⁺) was performed for 6 mice from each group. Images (\times 400, $n = 7$ /kidney) were taken randomly across the cortex of the UUO kidneys and noninjured CLKs, and positive cells were counted manually. Cell-cycle stages of myofibroblasts were calculated as follows: G0/G1 = all α -SMA⁺ cells – BrdU⁺/ α -SMA⁺ cells – p-H3⁺/ α -SMA⁺ cells; S = BrdU⁺/ α -SMA⁺ cells; G2/M = p-H3⁺/ α -SMA⁺ cells.

Cell-cycle stages of tubular cells were calculated as follows: G0/G1 = all tubular cells – BrdU⁺ tubular cells – p-H3⁺ tubular cells; S = BrdU⁺ tubular cells; G2/M = p-H3⁺ tubular cells. Quantification of the α -SMA⁺ surface area was performed by taking random cortical images (\times 200, $n = 7$ /kidney) of UUO kidneys and noninjured CLKs from each mouse ($n = 7$ vehicle vs. $n = 9$ darinaparsin) using the number of stained pixels per total pixels in Adobe Photoshop CS5 (Adobe Systems Inc.). All images were obtained by confocal (Nikon C1 Eclipse, Nikon) or standard microscopy (Nikon Eclipse 90i).

Fibrosis severity was scored at \times 400 magnification using a counting grid with 117 intersections. The number of grid intersections overlying trichrome-positive (blue) interstitial areas was counted and expressed as a percentage of all grid intersections. For this calculation, intersections that were in tubular lumen and glomeruli were subtracted from the total number of grid intersections.

To identify LacZ activity in kidney sections, PFA-fixed frozen sections were incubated in standard 5-bromo-4-chloro-3-indolyl- β -D-galactoside (X-gal) for 48 hours, counterstained with nuclear fast red, and mounted.

Cell culture experiments. All cell lines used in this study were ordered fresh from ATCC and routinely checked in our laboratory for mycoplasma contamination. 10T1/2 cells (ATCC) were cultured in Basal Medium Eagle (BME), supplemented with 10% FBS, penicillin and streptomycin, and 2 mmol/l glutamine (all from Gibco, Life Technologies). Shh-conditioned media were produced from supernatants of confluent Cos7 cells stably transfected with pcDNA3-N-Shh or pcDNA3 control plasmid. For Western blot experiments, cells were grown in 10-cm dishes, serum starved in 0.5% FBS for 12 hours, and then incubated with darinaparsin (0.5 μ M) or vehicle with either Shh-preconditioned medium or Cos7 control media (5 times, i.e., 2 ml preconditioned media in 8 ml BME containing 0.5% FBS) for 72 hours.

For cell-cycle analysis, cells were grown in 6-well plates until 50% confluency, serum starved in 0.5% FBS for 4 hours to synchronize the cell cycle, and then cultured for 48 hours in 10% FBS medium, together with 0.5 μ M darinaparsin or normal saline (vehicle). Before fixation, cells were incubated for 75 minutes in 10 μ M BrdU and stained according to the BD APC BrdU Flow Kit protocol (catalog 552598; BD Biosciences). Cells were analyzed by flow cytometry (FACSCanto II; BD Biosciences) within 1 hour of staining, and data were analyzed using FlowJo software, version 7.5.

siRNA-knockdown experiments. For siRNA experiments, cells were transfected with either siRNA directed against *Gli1* (Life Technologies, siRNA ID s66723; primer sequences: sense: 5'-GCAGGU-CUCCUAUCCUGAUTT-3', antisense: 5'-AUCAGGAUAGGAGAC-CUGCTG-3'); *Gli2* (Life Technologies, siRNA ID s66726; primer sequences: sense: 5'-GGAAAACUUCAACAAUACATT-3', antisense: 5'-UGUAUUGUUGAAGUUUCCAG-3'), or siRNA against both *Gli1* and *Gli2*. Scrambled siRNA was used as a negative control (catalog AM4611; Life Technologies), and Cy3-labeled siRNA directed against GAPDH (catalog AM4649; Life Technologies) was used as a positive control for the transfection. Transfection was performed with a final concentration of 5 nM of each siRNA, according to the manufacturer's instructions, using Lipofectamine RNAiMAX Transfection Reagent (catalog 3778075; Life Technologies). Seventy-two hours after transfection, cells were harvested for RNA or protein isolation. For cell-cycle analysis, cells were split 48 hours after transfection at a seeding density of 50%, and 24 hours after seeding, the cells were

incubated for 75 minutes with 10 μ M BrdU and subjected to cell-cycle analysis as described above.

Overexpression of *GLI2* by retroviral delivery. The RSF91.IRES.EGFP retroviral vector was a gift of Axel Schambach and Christopher Baum (both of Hannover Medical School). The vector was modified with a multiple cloning site containing the SbfI and MluI restriction enzyme sites. The full-length *Gli2* cDNA was provided by Hiroshi Sasaki (RIKEN database RDB 08065, gene ID 14633) (45). The *Gli2* cDNA was PCR amplified using Phusion Polymerase (catalog m0530; New England BioLabs Inc.), and an N-terminal HA tag, a 5' SbfI, and a 3' MluI site were added and the cDNA inserted into the multiple cloning site. Ecotropic retroviral particles were produced by calcium phosphate-based transient cotransfection of HEK293T cells with the retroviral constructs and packaging plasmid. Viral supernatants were collected 36–48 hours after transfection and 0.22 μ M filtered. Cell transduction was performed by incubating the cells with serial dilutions of the retroviral supernatants in the presence of 4 μ g/ml polybrene (catalog 107689; Sigma-Aldrich). Cell-cycle flow cytometric analysis was performed using DAPI instead of 7AAD for detection of DNA content due to the expression of viral GFP.

GLI2-darinaparsin-binding assay. Fresh human 293T/17 cells (HEK 293T/17; ATCC) were grown in a 10-cm cell culture dish until 80% confluent and transfected with pCS2-MT *GLI2* FL (Addgene plasmid 17648), provided by E. Roessler (48), using Lipofectamine 2000 (Life Technologies) according to the manufacturer's instructions. Cells were cotransfected with a myc-tagged GFP plasmid (pEGFP-C1-myc) as a control protein. pEGFP-myc was generated using pEGFP-C1 (Clontech Laboratories) and by addition of a myc tag at the BspEI and BamHI restriction sites. Seventy-two hours after transfection, the cells were treated for 12 hours with 0.5 μ M darinaparsin or vehicle in DMEM containing 10% FBS; thereafter, cells were resuspended in cold (4°C) PBS and washed twice with PBS. After centrifugation (220 g, 5 min), 1 ml IP lysis buffer (Thermo Scientific) plus proteinase inhibitor (catalog 1183617000T; Roche) were added to the cell pellet, and the suspension was homogenized using an insulin syringe. After centrifugation of the protein solution (13,500 g, 15 min), the supernatant was transferred into a fresh tube, an aliquot of 100 μ l was taken as an input control (Figure 4), and the solution was incubated with 50 μ l GST agarose beads (Pierce GST Agarose, catalog 20211; Thermo Scientific) for 4 hours on a rotator at 4°C. Thereafter, the bead-protein solution was centrifuged (2,400 g, 3 min), and the supernatant was taken as an outflow control (Figure 4). The agarose beads were washed 3 times by adding 1 ml of the above-mentioned IP lysis buffer containing proteinase inhibitors, followed by vortexing and centrifugation (2,400 g, 3 min), and the supernatant after each centrifugation was discarded. After 3 washes, the GST beads were cooked at 96°C for 7 minutes in 100 μ l Laemmli buffer (Bio-Rad). All protein samples (input, outflow, and the final GST bead purification solution) were analyzed by Western blotting with an Ab against c-myc (mouse mAb, 9E 10; Developmental Studies Hybridoma Bank [DSHB], University of Iowa, Iowa City, Iowa, USA), and immunoblotting against GFP was performed for confirmation.

Quantitative RT-PCR experiments. Kidney tissue or cell pellets were harvested and immediately snap frozen in liquid nitrogen. RNA was extracted according to the manufacturer's instructions using the RNeasy Mini Kit (QIAGEN), and 600 ng total RNA was reverse transcribed with iScript (Bio-Rad). Quantitative RT-PCR (qRT-PCR) was

carried out with iQ-SYBR Green SuperMix (Bio-Rad) and the Bio-Rad CFX96 Real Time System with the C1000 Touch Thermal Cycler. Cycling conditions were 95°C for 3 minutes, then 40 cycles of 95°C for 15 seconds and 60°C for 1 minute, followed by 1 cycle of 95°C for 10 seconds. *Gapdh* was used as a housekeeping gene. Data were analyzed using the $2^{-\Delta\Delta Ct}$ method. The primers used are listed in Supplemental Table 1 (mouse) and Supplemental Table 2 (human).

Western blot analysis. Kidney tissue was snap frozen in liquid nitrogen and stored at -80°C immediately after mice were killed. Tissue samples were homogenized in lysis buffer containing 10 mM HEPES, pH 7.4, 0.32 M sucrose, 2 mM EDTA, 1 mM DTT, 1 mM PMSF, and 1 protease inhibitor tablet per 10 ml lysis buffer (catalog 11836153001; Roche). Samples were sonicated, and the protein concentration was determined by the Bradford Assay using Protein Assay Dye (catalog 500-0006; Bio-Rad). Protein (10–40 μ g) from lysates was loaded on a 7.5% or 10% polyacrylamide gel and separated by SDS-PAGE. Proteins were transferred to an Immobilon membrane (EMD Millipore), blocked in 5% milk in PBS containing 0.1% Tween (PBST), and probed overnight at 4°C with the following primary Abs: mouse anti- α -SMA at 1:4,000 (catalog A2547; Sigma-Aldrich); rabbit anti-fibronectin at 1:4,000 (catalog ab23750; Abcam); rabbit anti-p21 at 1:200 (catalog sc-471; Santa Cruz Biotechnology Inc.); rabbit anti-p-Rb (71) at 1:1,000 (catalog 9307S, Ser780; Cell Signaling Technology); rat anti-GLI1 at 1:1,000 (catalog MAB3324; R&D Systems, http://www.antibodypedia.com/binder_details.php?binder_id=701973); goat anti-GLI2 at 1:500 (catalog AF3635; R&D Systems); rabbit anti-cyclin E at 1:200 (catalog sc-481; Santa Cruz Biotechnology Inc.); rabbit anti-cyclin A at 1:200 (catalog sc-751; Santa Cruz Biotechnology Inc.); rabbit anti-HA tag at 1:5,000 (catalog 3724; Cell Signaling Technology); mouse anti-c-myc (catalog 9E 10; DSHB); and rabbit anti-GAPDH at 1:4,000 (catalog A300-641A; Bethyl Laboratories). Following incubation with primary Abs, the blots were washed, probed with the respective HRP-conjugated secondary Abs at 1:5,000 (catalogs P0447, P0448, and P0450; Dako, Agilent Technologies) for 1 hour at room temperature, and then visualized using the Western Lightning ECL kit from PerkinElmer (catalog NEL100001EA). Quantification of Western blot bands was performed using ImageJ software (NIH).

Human kidney specimens. Human kidney specimens were obtained from 10 patients undergoing partial or total nephrectomy procedures for urologic indications (Supplemental Table 3). Nephrectomy specimens were immediately placed on ice, and within 15 minutes of surgical removal, three 5-mm cubes of tissue were cut from portions of non-neoplastic tissue and placed into 3 separate containers with specific preservatives (neutral buffered formalin, 4% PFA in PBS, or RNAlater [Life Technologies]). Trichrome-stained slides from formalin-preserved tissue were examined by a trained senior pathologist for semiquantitative assessment of cortical tubulointerstitial fibrosis.

Statistics. All results are reported as the mean \pm SEM. Comparison of 2 groups was performed using an unpaired *t* test or a Mann-Whitney *U* test where appropriate. For multiple group comparisons, ANOVA followed by Bonferroni's post-hoc correction was applied. Statistical analyses were performed using GraphPad Prism, version 5.0c (GraphPad Software Inc.). A *P* value of less than 0.05 was considered significant.

Study approval. All mouse experiments were approved by the IACUC of Harvard University. The human study was approved by the IRB of Brigham and Women's Hospital, and all patients provided written informed consent.

Acknowledgments

This work was supported by NIH grants DK088923 (to B.D. Humphreys) and DK104308 (to B.D. Humphreys and S.S. Waikar); by an Established Investigator Award of the American Heart Association (13EIA14650059, to B.D. Humphreys); by a fellowship from the RWTH Aachen University (to R. Kramann); and by grants from the Deutsche Forschungsgemeinschaft (Kr 40731-1, RKS 188/3-1, and SF Fl 828/1-1, to R. Kramann). We acknowledge support for

this project from the UAB-UCSD O'Brien Core Center for Acute Kidney Injury Research (NIH P30-DK079337).

Address correspondence to: Benjamin D. Humphreys, Renal Division, Department of Medicine, Washington University School of Medicine, Box 8126, 600 South Euclid Avenue, St. Louis, Missouri 63110, USA. Phone: 314.362.8233; E-mail: bhumphre@dom.wustl.edu.

- McCullough K, et al. Measuring the population burden of chronic kidney disease: a systematic literature review of the estimated prevalence of impaired kidney function. *Nephrol Dial Transplant*. 2012;27(5):1812-1821.
- McClellan WM, Plantinga LC. A public health perspective on CKD and obesity. *Nephrol Dial Transplant*. 2013;28(suppl 4):iv37-iv42.
- United States Renal Data System, 2014 Annual Data Report: Epidemiology of Kidney Disease in the United States. Vol. 2. Bethesda, Maryland, USA: National Institutes of Health, National Institute of Diabetes and Digestive and Kidney Diseases; 2014.
- Kramann R, DiRocco DP, Maarouf OH, Humphreys BD. Matrix-producing cells in chronic kidney disease: origin, regulation, and activation. *Curr Pathobiol Rep*. 2013;1(4):301-311.
- Kramann R, DiRocco DP, Humphreys BD. Understanding the origin, activation and regulation of matrix-producing myofibroblasts for treatment of fibrotic disease. *J Pathol*. 2013;231(3):273-289.
- Kramann R, et al. Perivascular gli1(+) progenitors are key contributors to injury-induced organ fibrosis. *Cell Stem Cell*. 2015;16(1):51-66.
- Hui CC, Angers S. Gli proteins in development and disease. *Annu Rev Cell Dev Biol*. 2011;27:513-537.
- Briscoe J, Theron PP. The mechanisms of Hedgehog signalling its roles in development disease. *Nat Rev Mol Cell Biol*. 2013;14(7):416-429.
- Robbins DJ, Fei DL, Riobo NA. The Hedgehog signal transduction network. *Sci Signal*. 2012;5(246):re6.
- Matisse MP, Epstein DJ, Park HL, Platt KA, Joyner AL. Gli2 is required for induction of floor plate and adjacent cells, but not most ventral neurons in the mouse central nervous system. *Development*. 1998;125(15):2759-2770.
- Litingtung Y, Chiang C. Specification of ventral neuron types is mediated by an antagonistic interaction between Shh and Gli3. *Nat Neurosci*. 2000;3(10):979-985.
- Park HL, et al. Mouse Gli1 mutants are viable but have defects in SHH signaling in combination with a Gli2 mutation. *Development*. 2000;127(8):1593-1605.
- Humke EW, Dorn KV, Milenkovic L, Scott MP, Rohatgi R. The output of Hedgehog signaling is controlled by the dynamic association between Suppressor of Fused and the Gli proteins. *Genes Dev*. 2010;24(7):670-682.
- Bai CB, Auerbach W, Lee JS, Stephen D, Joyner AL. Gli2, but not Gli1, is required for initial Shh signaling and ectopic activation of the Shh pathway. *Development*. 2002;129(20):4753-4761.
- Ding Q, et al. Diminished Sonic hedgehog signaling and lack of floor plate differentiation in Gli2 mutant mice. *Development*. 1998;125(14):2533-2543.
- Mo R, et al. Specific and redundant functions of Gli2 and Gli3 zinc finger genes in skeletal patterning and development. *Development*. 1997;124(1):113-123.
- Bai CB, Joyner AL. Gli1 can rescue the in vivo function of Gli2. *Development*. 2001;128(24):5161-5172.
- Yu J, Carroll TJ, McMahon AP. Sonic hedgehog regulates proliferation and differentiation of mesenchymal cells in the mouse metanephric kidney. *Development*. 2002;129(22):5301-5312.
- Aberger F, Ruiz IAA. Context-dependent signal integration by the Gli code: The oncogenic load, pathways, modifiers and implications for cancer therapy. *Semin Cell Dev Biol*. 2014;33:93-104.
- Fabian SL, et al. Hedgehog-Gli pathway activation during kidney fibrosis. *Am J Pathol*. 2012;180(4):1441-1453.
- Ding H, et al. Sonic hedgehog signaling mediates epithelial-mesenchymal communication and promotes renal fibrosis. *J Am Soc Nephrol*. 2012;23(5):801-813.
- Zhou D, et al. Sonic hedgehog is a novel tubule-derived growth factor for interstitial fibroblasts after kidney injury. *J Am Soc Nephrol*. 2014;25(10):2187-2200.
- Dennler S, et al. Induction of sonic hedgehog mediators by transforming growth factor- β : Smad3-dependent activation of Gli2 and Gli1 expression in vitro and in vivo. *Cancer Res*. 2007;67(14):6981-6986.
- Dennler S, Andre J, Verrecchia F, Mauviel A. Cloning of the human GLI2 promoter: transcriptional activation by transforming growth factor- β via SMAD3/ β -catenin cooperation. *J Biol Chem*. 2009;284(46):31523-31531.
- Xie J, et al. A role of PDGFR α in basal cell carcinoma proliferation. *Proc Natl Acad Sci U S A*. 2001;98(16):9255-9259.
- Li F, et al. Sonic hedgehog signaling induces vascular smooth muscle cell proliferation via induction of the G1 cyclin-retinoblastoma axis. *Arterioscler Thromb Vasc Biol*. 2010;30(9):1787-1794.
- Bigelow RL, Jen EY, Delehedde M, Chari NS, McDonnell TJ. Sonic hedgehog induces epidermal growth factor dependent matrix infiltration in HaCaT keratinocytes. *J Invest Dermatol*. 2005;124(2):457-465.
- Riobo NA, Lu K, Ai X, Haines GM, Emerson CP Jr. Phosphoinositide 3-kinase and Akt are essential for Sonic Hedgehog signaling. *Proc Natl Acad Sci U S A*. 2006;103(12):4505-4510.
- Ji Z, Mei FC, Xie J, Cheng X. Oncogenic KRAS activates hedgehog signaling pathway in pancreatic cancer cells. *J Biol Chem*. 2007;282(19):14048-14055.
- Schnidar H, et al. Epidermal growth factor receptor signaling synergizes with Hedgehog/Gli in oncogenic transformation via activation of the MEK/ERK/JUN pathway. *Cancer Res*. 2009;69(4):1284-1292.
- Stecca B, et al. Melanomas require HEDGEHOG-Gli signaling regulated by interactions between Gli1 and the RAS-MEK/AKT pathways. *Proc Natl Acad Sci U S A*. 2007;104(14):5895-5900.
- Pasca di Magliano M, Sekine S, Ermilov A, Ferris J, Dlugosz AA, Hebrok M. Hedgehog/Ras interactions regulate early stages of pancreatic cancer. *Genes Dev*. 2006;20(22):3161-3173.
- Wallace VA. Purkinje-cell-derived Sonic hedgehog regulates granule neuron precursor cell proliferation in the developing mouse cerebellum. *Curr Biol*. 1999;9(8):445-448.
- Dahmane N, Ruiz i Altaba A. Sonic hedgehog regulates the growth and patterning of the cerebellum. *Development*. 1999;126(14):3089-3100.
- Mann KK, Wallner B, Lossos IS, Miller WH Jr. Darinaparsin: a novel organic arsenical with promising anticancer activity. *Expert Opin Investig Drugs*. 2009;18(11):1727-1734.
- Tsimberidou AM, et al. A phase I clinical trial of darinaparsin in patients with refractory solid tumors. *Clin Cancer Res*. 2009;15(14):4769-4776.
- Izzi L, et al. Boc and Gas1 each form distinct Shh receptor complexes with Ptch1 and are required for Shh-mediated cell proliferation. *Dev Cell*. 2011;20(6):788-801.
- Mill P, et al. Sonic hedgehog-dependent activation of Gli2 is essential for embryonic hair follicle development. *Genes Dev*. 2003;17(2):282-294.
- Li Y, Zhang H, Choi SC, Litingtung Y, Chiang C. Sonic hedgehog signaling regulates Gli3 processing, mesenchymal proliferation, and differentiation during mouse lung organogenesis. *Dev Biol*. 2004;270(1):214-231.
- Vokes SA, Ji H, Wong WH, McMahon AP. A genome-scale analysis of the cis-regulatory circuitry underlying sonic hedgehog-mediated patterning of the mammalian limb. *Genes Dev*. 2008;22(19):2651-2663.
- Kim J, Lee JJ, Kim J, Gardner D, Beachy PA. Arsenic antagonizes the Hedgehog pathway by preventing ciliary accumulation and reducing stability of the Gli2 transcriptional effector. *Proc Natl Acad Sci U S A*. 2010;107(30):13432-13437.
- Beauchamp EM, et al. Arsenic trioxide inhibits human cancer cell growth and tumor development in mice by blocking Hedgehog/Gli pathway. *J Clin Invest*. 2011;121(1):148-160.
- Tian J, et al. Darinaparsin: solid tumor hypoxic cytotoxin and radiosensitizer. *Clin Cancer Res*.

- 2012;18(12):3366–3376.
44. Bansal N, Johnson Farley N, Wu L, Lewis J, Yousoufian H, Bertino JR. Darinaparsin inhibits prostate tumor initiating cells Du 145 xenografts as an inhibitor of hedgehog signaling. *Mol Cancer Ther*. 2015;14(1):23–30.
 45. Sasaki H, Nishizaki Y, Hui C, Nakafuku M, Kondoh H. Regulation of Gli2 and Gli3 activities by an amino-terminal repression domain: implication of Gli2 and Gli3 as primary mediators of Shh signaling. *Development*. 1999;126(17):3915–3924.
 46. Beauchamp EM, Uren A. A new era for an ancient drug: arsenic trioxide and Hedgehog signaling. *Vitam Horm*. 2012;88:333–354.
 47. Zhang XW, et al. Arsenic trioxide controls the fate of the PML-RAR α oncoprotein by directly binding PML. *Science*. 2010;328(5975):240–243.
 48. Roessler E, et al. A previously unidentified amino-terminal domain regulates transcriptional activity of wild-type and disease-associated human GLI2. *Hum Mol Genet*. 2005;14(15):2181–2188.
 49. Kramann R, Tanaka M, Humphreys BD. Fluorescence microangiography for quantitative assessment of peritubular capillary changes after AKI in mice. *J Am Soc Nephrol*. 2014;25(9):1924–1931.
 50. Diaz Z, et al. A novel arsenical has antitumor activity toward As₂O₃-resistant and MRP1/ABCC1-overexpressing cell lines. *Leukemia*. 2008;22(10):1853–1863.
 51. Garnier N, et al. The novel arsenical darinaparsin is transported by cystine importing systems. *Mol Pharmacol*. 2014;85(4):576–585.
 52. Garnier N, et al. The novel arsenical Darinaparsin circumvents BRG1-dependent, HO-1-mediated cytoprotection in leukemic cells. *Leukemia*. 2013;27(11):2220–2228.
 53. Machado AF, Hovland DN Jr, Pilafas S, Collins MD. Teratogenic response to arsenite during neurulation: relative sensitivities of C57BL/6J and SWV/Fnn mice and impact of the *slp1* allele. *Toxicol Sci*. 1999;51(1):98–107.
 54. DeSesso JM, Jacobson CF, Scialli AR, Farr CH, Holson JF. An assessment of the developmental toxicity of inorganic arsenic. *Reprod Toxicol*. 1998;12(4):385–433.
 55. Chaîneau E, Binet S, Pol D, Chatellier G, Meisinger V. Embryotoxic effects of sodium arsenite and sodium arsenate on mouse embryos in culture. *Teratology*. 1990;41(1):105–112.
 56. Riobo NA, Manning DR. Pathways of signal transduction employed by vertebrate Hedgehogs. *Biochem J*. 2007;403(3):369–379.
 57. Ribes V, Le Roux I, Rhinn M, Schuhbauer B, Dolle P. Early mouse caudal development relies on crosstalk between retinoic acid, Shh and Fgf signalling pathways. *Development*. 2009;136(4):665–676.
 58. Hao K, Tian XD, Qin CF, Xie XH, Yang YM. Hedgehog signaling pathway regulates human pancreatic cancer cell proliferation and metastasis. *Oncol Rep*. 2013;29(3):1124–1132.
 59. Sasaki K, Romer JT, Kimura H, Eberhart DE, Rice DS, Curran T. Medulloblastomas derived from Cxcr6 mutant mice respond to treatment with a smoothened inhibitor. *Cancer Res*. 2007;67(8):3871–3877.
 60. Samarzija I, Beard P. Hedgehog pathway regulators influence cervical cancer cell proliferation, survival and migration. *Biochem Biophys Res Commun*. 2012;425(1):64–69.
 61. Duman-Scheel M, Weng L, Xin S, Du W. Hedgehog regulates cell growth and proliferation by inducing Cyclin D and Cyclin E. *Nature*. 2002;417(6886):299–304.
 62. Nagao H, et al. Role of GLI2 in the growth of human osteosarcoma. *J Pathol*. 2011;224(2):169–179.
 63. Zhang D, Liu J, Wang Y, Chen J, Chen T. shRNA-mediated silencing of Gli2 gene inhibits proliferation and sensitizes human hepatocellular carcinoma cells towards TRAIL-induced apoptosis. *J Cell Biochem*. 2011;112(11):3140–3150.
 64. Plaisant M, Giorgetti-Peraldi S, Gabrielson M, Loubat A, Dani C, Peraldi P. Inhibition of hedgehog signaling decreases proliferation and clonogenicity of human mesenchymal stem cells. *PLoS One*. 2011;6(2):e16798.
 65. Lauth M, Bergstrom A, Shimokawa T, Toftgard R. Inhibition of GLI-mediated transcription and tumor cell growth by small-molecule antagonists. *Proc Natl Acad Sci U S A*. 2007;104(20):8455–8460.
 66. Shi T, et al. cDNA microarray gene expression profiling of hedgehog signaling pathway inhibition in human colon cancer cells. *PLoS One*. 2010;5(10):e13054.
 67. Moshai EF, et al. Targeting the hedgehog-glioma-associated oncogene homolog pathway inhibits bleomycin-induced lung fibrosis in mice. *Am J Respir Cell Mol Biol*. 2014;51(1):11–25.
 68. Humphreys BD, et al. Intrinsic epithelial cells repair the kidney after injury. *Cell Stem Cell*. 2008;2(3):284–291.
 69. Dunn SR, Qi Z, Bottinger EP, Breyer MD, Sharma K. Utility of endogenous creatinine clearance as a measure of renal function in mice. *Kidney Int*. 2004;65(5):1959–1967.
 70. Lauth M, Toftgard R. Non-canonical activation of GLI transcription factors: implications for targeted anti-cancer therapy. *Cell Cycle*. 2007;6(20):2458–2463.
 71. Chiariello M, Gomez E, Gutkind JS. Regulation of cyclin-dependent kinase (Cdk) 2 Thr-160 phosphorylation and activity by mitogen-activated protein kinase in late G1 phase. *Biochem J*. 2000;349(pt 3):869–876.